ORIGINAL PAPER

# Design and Application of Underground Mine Paste Backfill Technology

**Tikov Belem · Mostafa Benzaazoua**

**Abstract** This paper reviews the design and application of paste backfill in underground hard rock mines used as ground support for pillars and walls, to help prevent caving and roof falls, and to enhance pillar recovery for improved productivity. Arching after stope filling reduces vertical stress and increases horizontal stress distribution within the fill mass. It is therefore important to determine horizontal stress on stope sidewalls using various predictive models in the design of paste backfill. Required uniaxial compressive strength (UCS) for paste backfill depends on the intended function, such as vertical roof support, development opening within the backfill, pillar recovery, ground or pillar support, and working platform. UCS design models for these functions are given. Laboratory and backfill plant scale designs for paste backfill mix design and optimization are presented, with emphasis on initial tailings density control to prevent under-proportioning of binder content. Once prepared, paste backfill is transported (or pumped) and placed underground by pipeline reticulation. The governing elements of paste backfill transport are rheological factors such as shear yield stress, viscosity, and slump height (consistency). Different models (analytical, semi-empirical, and empirical) are given to predict the rheological factors of paste backfill (shear yield stress and viscosity). Following backfill placement underground, self-weight consolidation settlement, internal pressure build-up, the arching effect, shrinkage, stope volume, and wall convergence against backfill affect mechanical integrity.

**Keywords** Paste backfill · Mix design · Arching effect · Backfill strength · Backfill rheology

T. Belem (✉) · M. Benzaazoua
Department of Applied Sciences, Université du Québec en Abitibi-Témiscamingue (UQAT), 445, boul. de l'Université, Rouyn-Noranda, QC, Canada J9X 5E4
e-mail: tikou.belem@uqat.ca

M. Benzaazoua
Department of Applied Sciences, CRC on Integrated Management of Sulphidic Mine Tailings by Backfilling, UQAT, Rouyn-Noranda, Canada

## 1 Introduction

Underground cemented paste backfill (CPB) is an important component of underground stope extraction, and is commonly used in many cut-and-fill mines in Canada (e.g., Landriault et al. 1997; Naylor et al. 1997; Nantel 1998). As mining operations progress, paste backfill is placed into previously mined stopes to provide a stable platform for miners to work on and ground support for the walls of the adjacent adits by reducing the amount of open space that could potentially be filled by a collapse of the surrounding pillars (Barret et al. 1978). Underground paste backfill provides not only ground support to

pillars and walls, but also helps prevent caving and roof falls and enhances pillar recovery, thereby improving productivity (Mitchell 1989a, b; Coates 1981). Thus, the placement of paste backfill provides an extremely flexible system for coping with changes in ore body geometry that result in changes in stope width, dip, and length (Wayment 1978). The fill delivery method depends on the amount of energy required to deliver the backfill material underground, which in turn depends on the distribution cone (Arioglu 1983). Paste backfill is usually transported underground through reticulated pipelines.

Paste backfill is composed of mill tailings generated during mineral processing, mixed with additives such as Portland cements, lime, pulverized fly ash, and smelter blast furnace slag, which react as binding agents. Binding agents develop cohesive strength within CPB so that exposed fill faces become self-supporting when adjacent stopes are extracted. With the current fluctuations in metal prices, the survival of many mines depends on their ability to maximize productivity while minimizing costs. Backfilling costs in underground mining operations must be critically examined to identify potential cost savings (Stone 1993). Although paste backfilling is somewhat expensive, it is indispensable for most underground mines as it provides crucial ground support for mine safety and mining operations. Therefore, the fill should be cost-effective and capable of achieving the desired ground support and stability.

An analysis of fill stability must consider the geometric boundaries of the fill in terms of optimal economic use of CPB. Mine openings and exposed fill faces in large underground mines vary in shape from high and narrow to low and wide. Additionally, wall rock next to the backfill may be either steeply dipping or relatively flat-lying. The extraction sequence can be modified to reduce the number of CPB-filled stopes, or the stope geometries could be modified to reduce the required strength for CPB exposure (Mitchell 1989a, b; Stone 1993).

This paper reviews the design and application of paste backfill for underground ground support in mining operations, from preparation to placement underground. First, arching effects and their importance in filled stopes stability analysis is briefly introduced. This is followed by an overview of the design of required fill strength, from a review of current design methods. Next, optimal CPB-mix design (to reduce costs and improve fill strength) is discussed, followed by a discussion on the rheological properties of CPB. Finally, CPB delivery systems and underground placement are discussed.

## 2 Design of Horizontal Pressure on Filled Stope Sidewalls

In general, since self-weight stresses govern backfill design, the traditional design has been a free-standing wall requiring a uniaxial compressive strength (UCS) equal to the overburden stress at the bottom of the filled stope. In many cases, however, the adjacent rock walls actually help support the fill through boundary shear and arching effects. Therefore, backfill and rock walls may be mutually supporting (Mitchell 1989a). In backfilled stopes, when arching occurs (which is the case in many mines, depending on stope dimensions), the vertical pressure at the bottom of the filled stope is less than the weight of the overlying fill (overburden weight) due to horizontal pressure transfer, somewhat like a trap door (Martson 1930; Terzaghi 1943). This pressure transfer is due to frictional and/or cohesive interaction between fill and wall rock. When the pillars or stope walls begin to deform into the filled opening, the fill mass provides lateral passive resistance. Passive resistance is defined as the state of maximum resistance mobilized when force pushes against a fill mass and the mass exerts resistance to the force (Hunt 1986).

The pressure transferred horizontally to the sidewalls should be included in the required fill strength design. Horizontal pressures affected by fill arching are determined by five analytical or semi-analytical solutions that account for cohesion at the fill-sidewall interface and/or frictional sliding along the sidewalls. These solutions are Martson's model and its modified version, Terzaghi's model, Van Horn's model and our proposed model.

### 2.1 Martson's Cohesionless Model

Martson (1930) developed a two-dimensional arch solution to predict horizontal pressure ($\sigma_h$) at the bottom of an excavated trench (in kPa) along the excavation sidewalls, as follows:

$$\sigma_h = \frac{\gamma B}{2\mu'}\left[1 - \exp\left(-\frac{2K_a\mu'H}{B}\right)\right] \tag{1}$$

The corresponding vertical pressure $\sigma_v$ at the bottom of the excavation and the parameter $K_a$ are given as follows:

$$\sigma_v = \sigma_h/K_a \tag{2}$$

$$K_a = \tan^2(45° - \phi/2) \tag{3}$$

where $\gamma$ = fill bulk unit weight (kN/m$^3$); $B$ = stope width (m); $H$ = fill mass height (m); $\mu' = \tan\delta$ = sliding friction coefficient between fill and sidewalls ($\delta$ is the wall friction angle, generally assumed at between $\phi/3$ and $2\phi/3$, and ranging from 0° to 22°); $\phi$ = fill internal friction angle (degree); and $K_a$ = active earth pressure.

### 2.2 Modified Martson's Cohesionless Model

Aubertin et al. (2003) proposed a modified version of Martson's two-dimensional arch solution, originally defined using active earth pressure ($K_a$) and wall sliding friction ($\mu'$). The modified version to predict effective horizontal pressure ($\sigma'_{hH}$) along pillar sidewalls at a depth $H$ corresponding to the stope bottom is given as follows:

$$\sigma'_{hH} = \frac{\gamma B}{2\tan\phi'_f}\left[1 - \exp\left(-\frac{2KH\tan\phi'_f}{B}\right)\right] \tag{4}$$

Corresponding effective vertical pressure $\sigma'_{vH}$ at the stope bottom is given as follows:

$$\sigma'_{vH} = \sigma'_{hH}/K \tag{5}$$

where $\gamma$ = fill bulk unit weight (kN/m$^3$); $B$ = stope width (m); $H$ = fill height (m); $\phi'_f$ = fill effective internal friction angle (degree); and $K$ = earth pressure coefficient.

Earth pressure coefficient $K$ corresponds to three different states: $K_a$ (active), $K_0$ (at rest), and $K_p$ (passive), given by the following relationships:

$$\begin{cases} K = K_0 = 1 - \sin\phi'_f \\ K = K_a = \tan^2\left(45° - \phi'_f/2\right) \\ K = K_p = \tan^2\left(45° + \phi'_f/2\right) \end{cases} \tag{6}$$

where $K_0$ = earth pressure at rest or in place coefficient; $K_a$ = active earth pressure coefficient; and $K_p$ = passive earth pressure coefficient.

In Eq. 6, $K_0$ is Jaky's (1944) equation, generally used for loose sand, and may also be determined using the following relationship for perfectly elastic materials:

$$K_0 = \frac{v}{1 - v} \tag{7}$$

where $v$ = Poisson's ratio of the fill material, which must vary from 0.3 to 0.4, but is difficult to obtain for paste backfill materials.

According to Brooker and Ireland (1965), earth pressure at-rest coefficient for normally consolidated clays (i.e., plastic materials) is estimated by $K_0 = 0.95 - \sin\phi'$. Coefficient $K_0$ must vary from 0.4 to 0.6; $K_a$ must vary from 0.17 to 1.0; and $K_p$ must vary from 1.0 to 10. However, in a filled stope, the active earth pressure condition ($K_a$) seems improbable because the paste backfill has insufficient internal pressure to push out the stope walls. Thus, prevailing earth pressure conditions will probably be at rest and passive pressure only.

### 2.3 Terzaghi's Cohesive and Cohesionless Material Models

Terzaghi (1943) also developed a two-dimensional arch theory to predict horizontal pressure ($\sigma_h$) along pillar walls at the bottom of the excavation, given for a cohesive material by:

$$\sigma_h = \frac{(\gamma B - 2c)}{2\tan\phi}\left[1 - \exp\left(-\frac{2KH\tan\phi}{B}\right)\right] \tag{8a}$$

and for a cohesionless material as:

$$\sigma_h = \frac{\gamma B}{2\tan\phi}\left[1 - \exp\left(-\frac{2KH\tan\phi}{B}\right)\right] \tag{8b}$$

The corresponding vertical pressures $\sigma_v$ at stope bottom is given by:

$$\sigma_v = \sigma_h/K \tag{9}$$

and

$$K = \frac{1 + \sin^2\phi}{\cos^2\phi + 4\tan^2\phi} = \frac{1}{1 + 2\tan^2\phi} \tag{10}$$

where $K$ = earth pressure coefficient; $\gamma$ = fill bulk unit weight (kN/m$^3$); $c$ = fill cohesive strength (kPa); $B$ = stope width (m); $H$ = depth below fill toe (m); $\tan\phi$ = fill internal friction coefficient; and $\phi$ = fill internal friction angle (degree).

## 2.4 Three-dimensional Predictive Models

Van Horn (1963) proposed a theoretical 3D solution for vertical stress at a depth $h$ below the surface in a box of width $B$ and breath $L$, in which the interface friction angle between backfill and walls $\delta$ is estimated by following equation:

$$\sigma_v = \frac{\gamma}{2k_r \tan\delta}\left(\frac{BL}{B+L}\right)\left[1 - \exp\left(-2k_r \tan\delta \frac{2h(B+L)}{BL}\right)\right]$$
(11)

where $\gamma$ = fill bulk unit weight (kN/m$^3$); $h$ = fill height in the stope below the surface (m); $B$ = stope width; $L$ = stope strike length (m); and $k_r = \sigma_h/\sigma_v$; $\delta$ = interface friction angle (°) between backfill and stope wall.

Belem et al. (2004) proposed a three-dimensional model that implicitly takes into account arching effects to predict horizontal pressures at the stope floor ($\sigma_h$): both longitudinal pressure $\sigma_x$ (across ore body) and transverse pressures $\sigma_y$ (along ore body). The model is given as follows:

$$\sigma_h = \omega\gamma H\left(\frac{H}{B+L}\right) \times \left[1 - \exp\left(-\frac{2H}{B}\right)\right]$$
(12)

Corresponding vertical pressure $\sigma_v(= \sigma_z)$ at the stope bottom is given as follows:

$$\sigma_v = 0.185\gamma H\left(\frac{H}{B+L}\right) \times \left[1 - \exp\left(-\frac{2H}{B}\right)\right] = \sigma_z$$
(13)

where $\gamma$ = fill bulk unit weight (kN/m$^3$); $H$ = fill height in the stope (m); $B$ = stope width; $L$ = strike length of stope (m); and $\omega$ = directional constant, which is 1 for pressure across ore body ($\sigma_h = \sigma_x$) and 0.185 for pressure along ore body ($\sigma_h = \sigma_y$).

## 3 Paste Backfill Required Strength Design

The required strength for paste backfill depends on the intended function. To provide adequate ground support, the required uniaxial/unconfined compressive strength (UCS) of the fill should be at least 5 MPa, whereas for free-standing fill applications, UCS is commonly lower than 1 MPa (Stone 1993; Li et al. 2002). A typical vertical exposure measures 4–6 m wide by 30–45 m high. A UCS of 100 kPa is

commonly adopted as the liquefaction potential limit (Grice 2001; le Roux et al. 2002). Required static strength for paste without exposures may be arbitrarily selected at 200 kPa (e.g., Li et al. 2002). Previous work indicates that fill mass UCS varies from 0.2 MPa to 4 MPa, while surrounding rock mass UCS varies from 5 MPa to 240 MPa (e.g., Grice 1998; Revell 2000).

### 3.1 Vertical Backfill Support

The mechanical effects of fill differ from those of primary ore pillars. Research and in situ testing have shown that fill is incapable of supporting the total weight of overburden ($\sigma_v = \gamma H$), and acts as a secondary support system only (Cai 1983). The fill modulus of elasticity varies from 0.1 GPa to 1.2 GPa, while the surrounding rock mass elasticity varies from 20 GPa to 100 GPa. As discussed by Donavan (1999), we may assume that any vertical loading is a result of roof deformation (Fig. 1), and that design UCS can be estimated by the following relationship:

$$UCS_{design} = (E_p\varepsilon_p)FS = E_p\left(\frac{\Delta H_p}{H_p}\right)FS$$
(14)

where $E_p$ = rock mass or pillar elastic modulus; $\varepsilon_p$ = pillar axial strain; $\Delta H_p$ = strata deformation
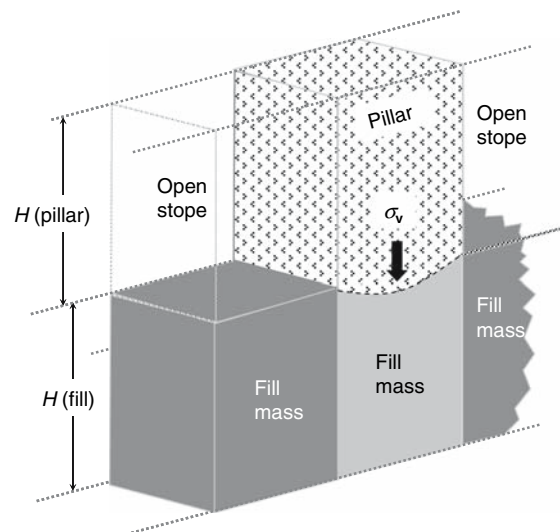


**Fig. 1** Schematic showing vertical loading on the backfill block next to a pillar

$(m)$; $H_p$ = strata initial height (m); and $FS$ = factor of safety.

When stope walls deform before backfilling, maximum load probably never approaches total weight of the deformed overlying strata (Donavan 1999), and design UCS can be estimated by the following relationship:

$$UCS_{design} = k(\gamma_p H_p)FS \qquad (15)$$

where $k$ = scaling constant, which must vary from 0.25 to 0.5; $\gamma_p$ = strata unit weight (kN/m³); $H_p$ = strata height below surface (m); and $FS$ = factor of safety.

Numerical modeling is also used to determine the required stiffness or strength of CPB to prevent subsidence due to roof deformation. Results are very useful to indicate the required paste backfill amount. Modeling is performed with either the FLAC (2D and 3D) or Phase$^{2D}$ code. Physical modeling, such as using a centrifuge, offers an alternative to numerical modeling, but its application is usually limited to simple gravitational models without high tectonic or in situ horizontal stresses (Stone 1993).

## 3.2 Development Opening Through Backfill Mass

When a gallery has to be opened through the paste backfill to access a new ore body (Fig. 2), safe design criteria must be applied. A conservative design considers a fill mass as more than two contiguously exposed faces after blasting adjacent pillars or stopes. Consequently, the walls confining the fill are removed and the fill mass is subjected to gravity loading similar to a laboratory sample subjected to the uniaxial compression test (Yu 1992). Design UCS is estimated by the following relationship:

$$UCS_{design} = (\gamma_f H_f)FS \qquad (16)$$

where $\gamma_f$ = fill bulk unit weight (kN/m³); $H_f$ = fill height (m); and $FS$ = factor of safety.

## 3.3 Pillar Recovery

To maximize ore recovery, it is very common to recycle mine pillar ore after primary ore recovery.
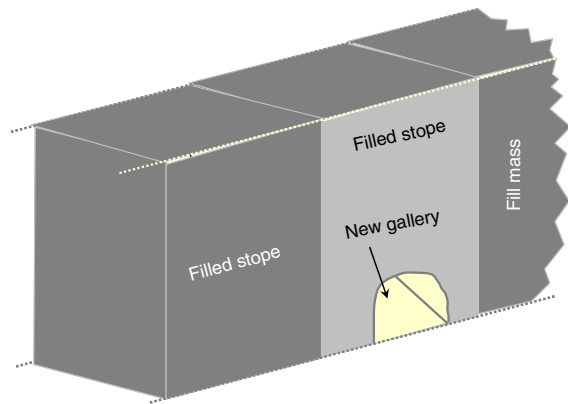


**Fig. 2** Development opening through a backfill mass

During the process, large vertical heights of paste backfill mass may be exposed. For delayed paste backfill, as in open stoping operations, the fill must be stable when free-standing wall faces are exposed during pillar recovery (Fig. 3). In addition the fill must have sufficient strength to remain free-standing during and after the pillar extraction process by resisting blast effects. Figure 3 illustrates a failure mechanism that could potentially occur after a stope blast. Depending on the mining schedule, moderate CPB strength (UCS < 1 MPa) may be required in the short term (Hassani and Archibald 1998).

In the absence of numerical modeling, many mine engineers rely on two-dimensional limit equilibrium analyses along with a calculated factor of safety (FS) to determine fill exposure stability. The typical result is an over-conservative estimate of limiting or critical strength (Stone 1993), which increases backfill
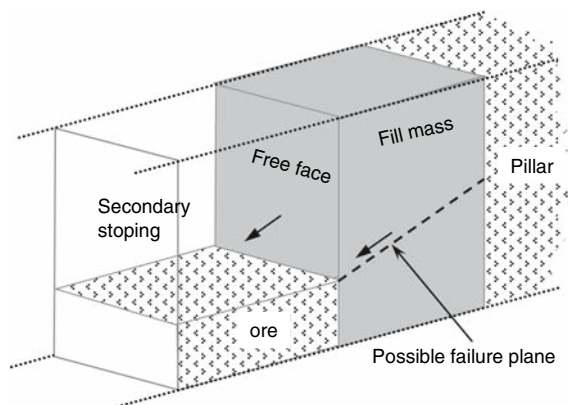


**Fig. 3** Fill mass failure mechanism during secondary stope extraction

operational costs. In recent years, however, 2D- and pseudo-3D empirical models have been developed to account for arching effects, cohesion, and friction along sidewalls (Mitchell et al. 1982; Smith et al. 1983; Arioglu 1984; Mitchell 1989a, b; Mitchell and Roettger 1989; Chen and Jiao 1991; Yu 1992). These design methods use the concept of a confined fill block surrounded by wall rock.

### 3.3.1 Case of More than Two Exposed Faces

Equation 16 should be used if there are more than two contiguously exposed faces after blasting adjacent pillars or stopes (Fig. 4).

### 3.3.2 Case of Narrowly Exposed Fill Face

This design method accounts for arching effects on confined fill by adjacent stope walls (Fig. 5) using Terzaghi's arching model (Eq. 9). Based on 2D finite element modeling, Askew et al. (1978) proposed the following formula to determine design fill compressive strength:

$$UCS_{design} = \frac{1.25B}{2K \tan \phi}\left(\gamma - \frac{2c}{B}\right)$$
$$\times \left[1 - \exp\left(-\frac{2HK \tan \phi}{B}\right)\right] FS \quad (17)$$

where $B$ = stope width; $K$ = fill pressure coefficient (see Eq. 10); $c$ = fill cohesive strength (kPa); $\phi$ = fill internal friction angle (degree); $\gamma$ = fill bulk unit
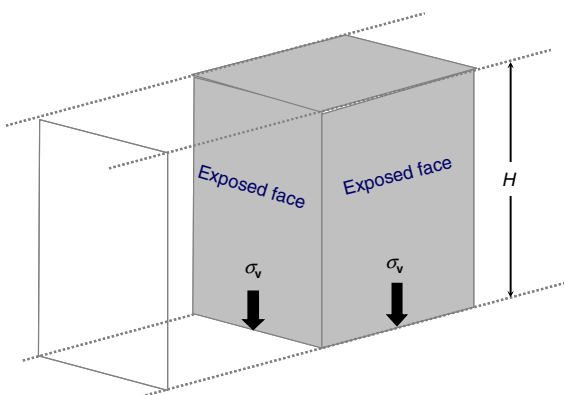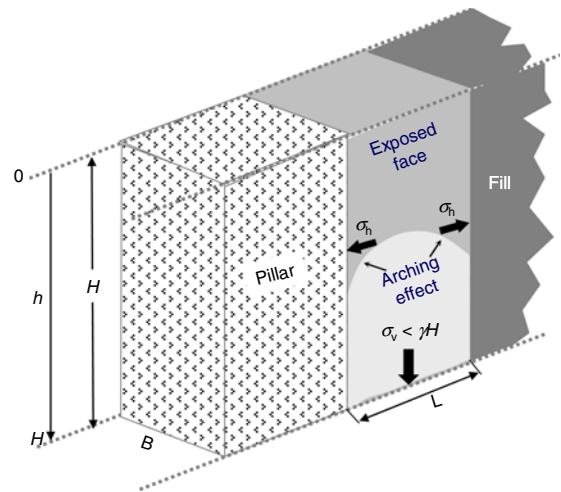


**Fig. 5** Schematic illustration of a stability analysis of a narrowly exposed fill face

weight (kN/m$^3$); $H$ = fill height (m); and $FS$ = factor of safety.

Fill cohesion ($c$) and its angle of internal friction ($\phi$) are obtained from triaxial tests performed on laboratory or in situ backfill samples.

### 3.3.3 Case of Exposed Frictional Fill Face

This design addresses an exposed fill where the two opposite sides of the fill are against stope walls (Fig. 6). Assuming shear resistance between fill and stope walls due to fill cohesion, design UCS is [estimated] by the following relationship (Mitchell et al. 1982):
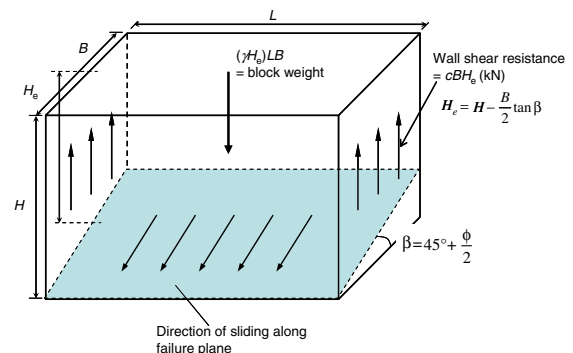


**Fig. 4** Schematic of a fill mass showing three exposed vertical faces



**Fig. 6** Confined block with shear resistance mechanism (from Mitchell et al. 1982)

$$UCS_{design} = \frac{(\gamma L - 2c)}{L}\left[H - \frac{B}{2}\tan\left(45° + \frac{\phi}{2}\right)\right]$$
$$\times \sin\left(45° + \frac{\phi}{2}\right)FS \tag{18}$$

where $\gamma$ = fill bulk unit weight (kN/m³); $c$ = fill cohesive strength (kPa); $L$ = stope strike length (m); $B$ = stope width (m); $H$ = total fill height (m); $\phi$ = fill internal friction angle (degree); and $FS$ = factor of safety.

Again, fill cohesion ($c$) and its angle of internal friction ($\phi$) are obtained from triaxial tests performed on laboratory or in situ backfill samples.

### 3.3.4 Case of Exposed Frictionless Fill Face

The compressive strength of paste backfill is mainly due to binding agents, and any strength contributed by friction is considered negligible in the long term (i.e., $\phi \approx 0$). For a frictionless material (Fig. 7), cohesion is assumed at half the UCS ($c = UCS/2$). Thus, design UCS is determined by the following relationship, proposed by Mitchell et al. (1982):

$$UCS_{design} = \frac{\gamma L\left(H - \frac{B}{2}\right)}{\frac{L}{FS\sin 45°} + \left(H - \frac{B}{2}\right)} = \frac{\gamma L\left(H - \frac{B}{2}\right)FS\sqrt{2}}{2L + \left(H - \frac{B}{2}\right)FS\sqrt{2}} \tag{19}$$

where $\gamma$ = fill bulk unit weight (kN/m³); $c$ = fill cohesive strength (kPa); $B$ = stope width (m); $L$ = stope strike length (m); $H$ = fill height (m); and $FS$ = factor of safety (ca. 1.5).
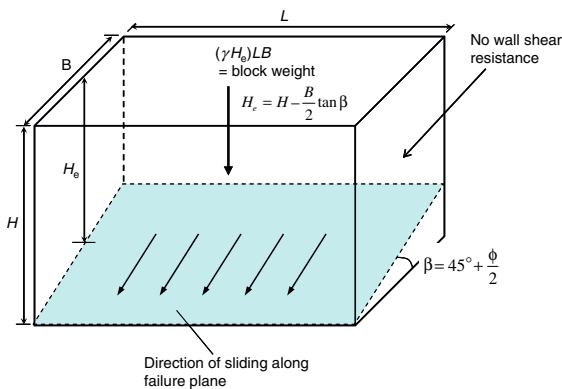
The stability of free-standing backfill (Fig. 7) can also be determined from physical model tests such as centrifugal modeling tests. Mitchell (1983) proposed a formula derived from Eq. 19, where $B = 0$ and $FS = \sqrt{2}$, and which is used to determine design UCS as follows:

$$UCS_{design} = \frac{\gamma LH}{L + H} = \frac{\gamma H}{\left(1 + \frac{H}{L}\right)} \tag{20}$$

and for a factor of safety other than 1, Eq. 20 is given as follows:

$$UCS_{design} = \frac{(\gamma LH)FS}{L + H} = \frac{(\gamma H)FS}{\left(1 + \frac{H}{L}\right)} \tag{21}$$

where $\gamma$ = fill bulk unit weight (kN/m³); $L$ = stope strike length (m); $H$ = fill height (m); and $FS$ = factor of safety.

### 3.4 Ground Support

After passive resistance has been mobilized by the fill, the strength increase in the surrounding pillars is equal to the passive fill pressure. Thus, the main stabilizing effect of the fill is to provide increased lateral confining pressure to the pillars (Fig. 8). Compressive strength of the pillar increases according to the following formula (Guang-Xu and Mao-Yuan 1983):

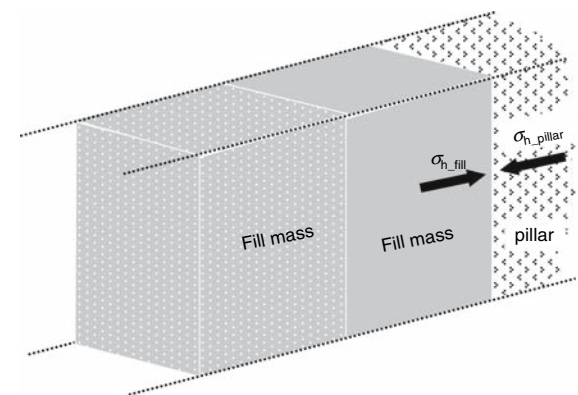$$UCS_{cp} = UCS_{up} + [(\gamma_f H_f)K_{a-f}]K_{p-p} \tag{22}$$

and



**Fig. 7** Confined block with no shear resistance mechanism of frictionless fill (adapted from Mitchell et al. 1982)



**Fig. 8** Schematic diagram of a pillar confined by the fill mass

$$K_{a-f} = \tan^2(45° - \phi_f/2) \tag{23a}$$

$$K_{p-p} = \tan^2(45° + \phi_p/2) \tag{23b}$$

where $UCS_{cp}$ = confined pillar compressive strength (kPa); $UCS_{up}$ = unconfined pillar strength before stope filling (kPa); $\gamma_f$ = fill bulk unit weight (kN/m$^3$); $H_f$ = paste backfill (m); $\phi_f$ = fill internal friction angle (degree); $\phi_p$ = pillar internal friction angle (degree); $K_{a-f}$ = fill active pressure coefficient; and $K_{p-p}$ = passive pressure coefficient of the pillar.

### 3.5 Working Platform

For cyclic backfill operations, as in cut-and-fill stoping, each fill must serve as a platform for both mining equipment and personnel, and typically requires high strength development in the short-term. A standard bearing capacity relationship, developed with civil engineering methods for shallow foundation design, would be suitable for this type of backfill. Fill top surface bearing capacity $Q_f$ (kPa) is determined using Terzaghi's expression, modified by Craig (1995), as follows:

$$Q_f = 0.4\gamma B N_\gamma + 1.2 c N_c \tag{24}$$

Bearing factors $N_\gamma$ (developed by Hansen 1968) and $N_c$ are given by the following relationships:

$$N_\gamma = 1.8(N_q - 1)\tan\phi \tag{25a}$$

$$N_c = \frac{(N_q - 1)}{\tan\phi} \tag{25b}$$

and

$$N_q = \tan^2(45° + \phi/2)\exp(\pi\tan\phi) \tag{25c}$$

where $N_\gamma$ = unit weight bearing capacity factor; $N_c$ = cohesion bearing capacity factor; $N_q$ = surcharge bearing capacity factor; $\gamma$ = fill bulk unit weight (kN/m$^3$); $c$ = fill cohesive strength (kPa); $B$ = width of square footing at surface contact position (m); and $\phi$ = fill internal friction angle (degree).

Equation 24 assumes that the backfill bearing is supported by a square footing, which is reasonable represented by the footprint of a mine vehicle tire (Hassani and Bois 1992; Hassani and Archibald 1998). For mine vehicles (Fig. 9), contact width $B$
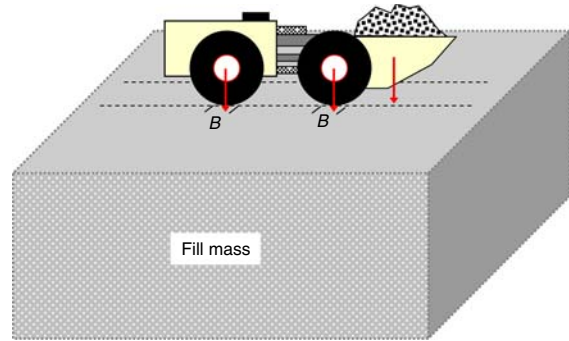


**Fig. 9** Schematic diagram of a working platform (adapted from Hassani and Bois 1992)

corresponds to tire contact width, and is determined by the following relationship (Hassani and Bois 1992):

$$B = \sqrt{\frac{F_t}{p}} \tag{26}$$

where $F_t$ = tire loading force (kN); and $p$ = tire air pressure (kN/m$^2$).

## 4 Optimizing Paste Backfill Mix Designs

Once required strength has been determined, mix variables are optimized to provide the desired mix that achieves target strength and minimum cementitious usage. Mix variables considered include binder content $B_{w\%}$ (by dry mass of tailings) and binder type, tailings particle size distribution (PSD) and mineralogy, mix solids concentration by mass ($C_{w\%}$) or volume ($C_{V\%}$), and mixing water geochemistry. To design a certain uniaxial compressive strength ($UCS_{design}$), variables are adjusted to produce an optimal mix design (Stone 1993; Benzaazoua et al. 1999, 2000, 2003; Benzaazoua et al. 1999, 2000; Benzaazoua and Belem 2000; Fall and Benzaazoua 2003; Kesimal et al. 2003; Yilmaz et al. 2004).

The other essential requirement is that the backfill must be economical. Typical backfill costs vary from $2 CDN/m$^3$ to $20 CDN/m$^3$ for paste backfill, depending on the service required. These costs wield a significant impact on the mine's operating costs. Paste backfill costs alone are typically between 10% and 20% of total mine operating costs, with binder agents accounting for up to 75% of backfill costs (Grice 1998; Fall and Benzaazoua 2003).

## 4.1 Laboratory Optimization of CPB Mix Designs

Optimizing CPB mix designs reduces binder usage and offers significant cost savings (e.g., Benzaazoua and Belem 2000; Benzaazoua et al. 2002; Fall and Benzaazoua 2003). Figure 10 shows the main components affecting the final quality of paste backfill such as binding agents, tailings characteristics (specific gravity, mineralogy, particle size distribution), and finally, mixing water chemistry and geochemistry (sulphate concentration, pH, Eh, Electrical conductivity). Each component plays an important role in backfill transportation and delivery, placement, and long-term hardening (Benzaazoua et al. 2002).

### 4.1.1 Binder Types and Content

Hardening of CPB occurs as bonds are formed between fill particles at grain contact points. Several types of binding agents are used, but the most common is ordinary Portland cement (CEM I, OPC, Type 10, or Type I). Sulphate resistant Portland cement (SRPC, Type 50, or Type V) is sometimes used, although it is much more expensive than OPC. Admixtures with pozzolanic materials are often used to curb costs by reducing the amount of Portland cement needed for hardening. Pulverized fly ash (PFA) and smelter ground granulated blast furnace slags (GGBFS) are the most popular pozzolans used as admixtures (e.g., Douglas and Malhotra 1989). They can be used alone or blended with OPC (*binding agent = x*OPC + (1 − x)*Admixture*) to activate reactivity.
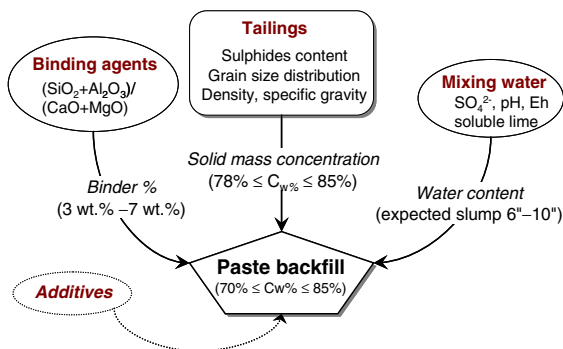


**Fig. 10** Schematic diagram of various paste backfill components (adapted from Benzaazoua et al. 2002)

Typical binder content $B_{w\%} (= 100 \times M_{binder}/M_{dry-tailings})$ varies from 3 wt.% to 7 wt.% (by dry mass of tailings). Solids mass concentration $C_{w\%}$(wt.%) is given as follows:

$$C_{w\%} = \frac{100 \times M_{solid}}{M_{water} + M_{solid}}$$
$$= \frac{100 \times \left(M_{dry-tailings} + M_{dry-binder}\right)}{M_{water} + M_{dry-tailings} + M_{dry-binder}} \quad (27)$$

where $M$ = mass of the substance (in g, kg, or tonne).

Corresponding volumetric binder content $B_{v\%}$ (v/v%) and solids concentration $C_{v\%}$ (v/v%) are given as follows:

$$B_{v\%} = \frac{V_{binder}}{V_{tailings}} \times 100 = B_{w\%}\left(\frac{\rho_{s-t}}{\rho_{s-b}}\right) \quad (28)$$

and

$$C_{v\%} = \frac{V_{solid}}{V_{bulk}} \times 100 = \frac{\rho_{d-f}}{\rho_{s-f}} \times 100 \quad (29)$$

where $V_{binder}$ = volume of binder; $V_{tailings}$ = volume of dry tailings; $V_{solid}$ = volume of dry tailings and binder; $V_{bulk}$ = volume of pastefill; $B_{w\%}$ = binder content (wt.%); $\rho_{s-t}$ = specific density of tailing grains; $\rho_{s-b}$ = specific density of binder grains; $\rho_{d-f}$ = dry density of pastefill; and $\rho_{s-f}$ = specific density of pastefill grains. Volumes are in cm$^3$ or m$^3$; densities are in g/cm$^3$, kg/m$^3$ or tonne/m$^3$.

From the known solids concentration by mass of paste backfill ($C_{w\%}$), the corresponding anhydrous binder concentration (%binder) and tailings grains concentration (%tailings) are calculated using the following formulae:

$$\%binder = C_{w\%}\left(\frac{B_{w\%}}{100 + B_{w\%}}\right) \quad (30a)$$

and

$$\%tailings = \left(\frac{C_{w\%}}{100 + B_{w\%}}\right) \times 100 = C_{w\%} - \%binder \quad (30b)$$

where $C_{w\%}$ = solids concentration by mass of CPB (%); and $B_{w\%}$ = binder content by dry mass of tailings (wt.%).

Numerous laboratory test results have reported that, for a given curing time, paste backfill strength is proportional to binder content $B_{w\%}$ (Fig. 11). However, this relationship is specific to each mine
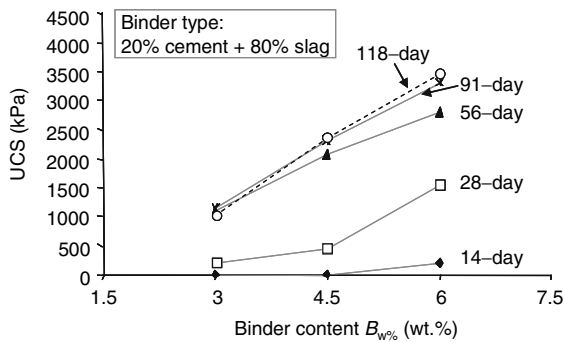
**Fig. 11** Typical variation of UCS with binder content at different curing times (from Benzaazoua et al. 2000)



**Fig. 12** Effect of mixing water on strength development within paste backfill mixtures with mine A tailings (from Benzaazoua et al. 2002)

(e.g., Benzaazoua et al. 1999, 2000; Belem et al. 2000; Benzaazoua and Belem 2000; Benzaazoua et al. 2002, 2004). Recent results have shown that the hardening process within paste backfill material is due not only to binder hydration but also precipitation of hydrated phases from the paste pore water (Benzaazoua et al. 2004).

### 4.1.2 Mixing Water and its Quality

Water is required to ensure proper hydration of the binding agents. Without adequate binder hydration, the fill cannot meet required strength and stiffness. Moreover, since additional water is usually required to pump the paste backfill underground, the volumetric water content of paste backfill is always far in excess of the OPC hydration requirements (as is the case for blends of OPC with SRPC, PFA or GGBFS). The main concern is therefore the water's pH and sulphate salts content. Acidic water and sulphate salts attack cementitious bonds within the fill, leading to loss of strength, durability, and stability (e.g., Mitchell et al. 1982; Lawrence 1992; Wang and Villaescusa 2001; Benzaazoua et al. 2002, 2004).

Figure 12 illustrates that, when using blended Portland cement/GBFS binder with the same tailings sample mixed with three different waters, CPB hardening is slow for all three waters at 14-day curing. Beyond that curing time and at 28-day curing, UCS reaches a maximum value for sulphate-free waters (tap and lake water), or 600 kPa higher than a mix with sulphate-rich Mine A process water (Benzaazoua et al. 2002).
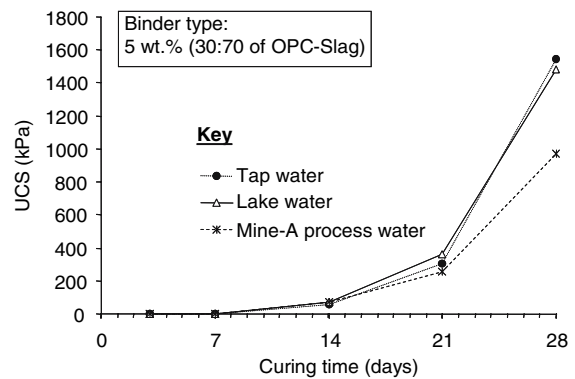
### 4.1.3 Binder Hydration Process

According to dissolution test data performed on the general use Portland cement (OPC or Type I) and blast furnace slag binders (Benzaazoua et al. 2004), a linear regression equation was derived for the calculation of percentage (by weight, wt.%) of dissolved binder $D_b$ as a function of water-to-cement ratio ($w/c$): $D_b(\text{wt.\%}) = 3.125 \times (w/c) + 3.3125$ (Belem et al. 2007). Figure 13 is a schematic illustration of the hydration process in cemented paste backfill materials. This figure illustrates that paste backfill hardening occurs in two main stages: *dissolution/hydration*, dominated by the dissolution and hydration processes, and *hydration/precipitation*, characterized by the precipitation process and direct hydration of binding agents (Benzaazoua et al. 2004).

Figure 14 presents a diagram of all possible stages in the hydration process of a paste backfill with tailings containing sulphide minerals (pyrite, pyrrhotite) and the mix solution containing sulphates. It reveals that, immediately after paste mixing with the binding agent, OH⁻ anions are released, which buffer the solution at a pH varying between 12 and 13. Consequently, the *dissolution/hydration* and *hydration/precipitation* phases take place successively. This hardening process first involves the formation of primary ettringite, followed by portlandite formation. At mid- and long-term hydration, C–S–H phases are formed, which largely contribute to paste backfill strength development. Depending on initial sulphate content, the formed portlandite could possibly react to gypsum.

**Fig. 13** Schematic diagram of volumetric proportions in hardening process of paste backfill having $w/c = 7$ (adapted from Benzaazoua et al. 2004)
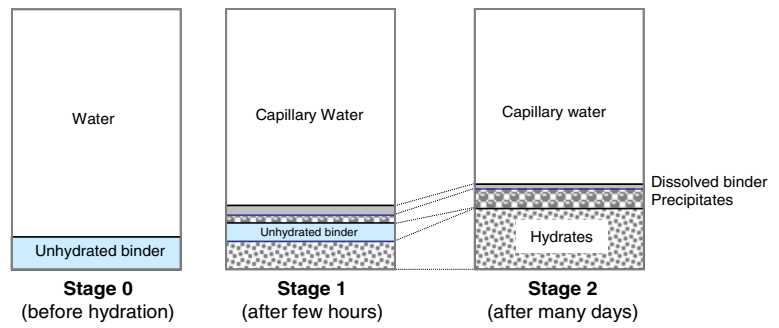


Bellmann et al. (2006) demonstrated that portlandite reacts to gypsum at a minimal sulphate concentration of approximately 1,400 mg/l (pH = 12.45). Their results suggest that, at common moderate concentrations of up to 1,500–3,000 mg/l of sulphate, gypsum formation is either not possible or cannot lead to damage, since supersaturation and swelling pressure are very low. At low sulphate concentrations, minor amounts of alkali ions already present in the pore solution act to protect the microstructure from the destructive process of gypsum formation.

Sulphide mineral (pyrite, pyrrhotite, arsenopyrite) oxidation has been shown to produce increased acidity (pH drops), metal remobilisation, sulphate ions release, and dissolution of formed hydrates. For example, when pH < 12 (stability limit of portlandite), potential outcomes are partial or total dissolution of portlandite ($Ca(OH)_2$), release of calcium from the formed hydrates (decalcification of C–S–H phases), and increased micro and mesoporosity.

The presence of sulphates in the mixture plays various other roles, depending on concentration (Benzaazoua et al. 2004). When sulphate content is between 200 and 8,000 mg/l, an inhibition stage of paste backfill hydration is likely. For sulphate concentrations ranging between 8,000 and 10,000 mg/l, precipitation of secondary gypsum is probable, and contributes to develop paste backfill strength. For sulphate content higher than 10,000 mg/l, sulphate attack, characterized by massive and harmful precipitation of secondary gypsum and ettringite (swelling phases), is expected. This excess volume is unable to fill capillary pores, as gypsum and ettringite crystals become much larger than the pores, which leads to expansion and microcracking of cured paste backfill. The outcome is loss of initially developed strength.

### 4.1.4 Paste Backfill Mixing Procedure

As mentioned above, a quantity of water is added to the tailings and binding agent and mixed for approximately 5–7 min in a concrete mixer. Due to the wide variety of tailings types, the resultant paste backfill mixture typically contains between 63 wt.% and 85 wt.% solids concentration by mass $C_{w\%}$, depending on initial tailings solid particles density $(2.8 \leq \rho_{s-t} \leq 4.7)$, binder content $(B_{w\%})$, and

**Fig. 14** Schematic diagram of paste backfill hydration process
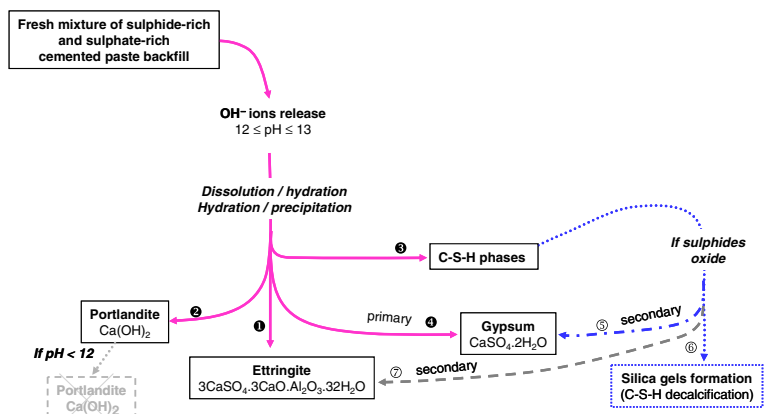
water-to-cement ratio ($W/C$), given by the following relationships:

$$C_{w\%} = \frac{100 \times (100 + B_{w\%})}{100 + B_{w\%}\left(1 + \frac{W}{C}\right)} \tag{31a}$$

and

$$\frac{W}{C} = \frac{w(\%)}{100}\left(\frac{100}{B_{w\%}} + 1\right) = \left(\frac{100 - C_{w\%}}{C_{w\%}}\right)\left(\frac{100}{B_{w\%}} + 1\right) \tag{31b}$$

where $C_{w\%}$ = solids concentration by mass of CPB (%); $B_{w\%}$ = binder content by mass (wt.%); $W/C$ = water-to-cement ratio; $w(\%)$ = water content of the final backfill mix (in percent), given by:
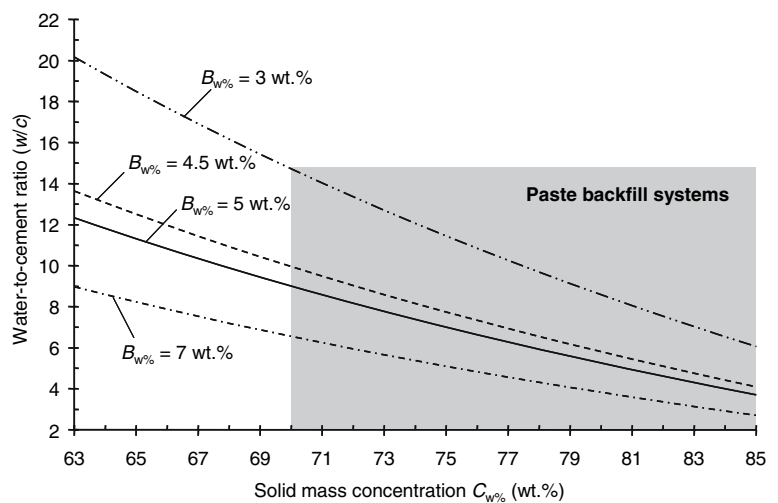
$$w(\%) = \frac{100 \times M_{water}}{M_{dry-solid}} \tag{32}$$

Considering the range of variation in $C_{w\%}$ (from 63 wt.% to 85 wt.%) and $B_{w\%}$ (from 3 wt.% to 7 wt.%) encountered in the mining industry, $W/C$ varies from 2.7 to 20.2 (compared to the approximately 0.5 $W/C$ used in the concrete industry). Figure 15 presents a typical variation of water-to-cement ratio $W/C$ for four different binder contents commonly used in the mining industry. The equivalent volumetric solids concentration $C_{v\%}$ is calculated by the following formula:

$$C_{v\%} = 100(1 - n) = \frac{100}{1 + e} \tag{33a}$$

and for backfill solids concentration by mass ($C_{w\%}$) as follows:

$$C_{v\%} = C_{w\%}\left(\frac{\rho_{bulk-f}}{\rho_{s-f}}\right) = \frac{100}{1 + \left(\frac{100}{C_{w\%}} - 1\right) \times \frac{G_{s-f}}{S_r}} \tag{33b}$$

where $\rho_{bulk-f}$ = pastefill bulk density (kg/m$^3$); $\rho_{s-f}$ = pastefill solid particles (tailings + binder) specific density (kg/m$^3$); $n$ = CPB porosity ($V_{void}/V_{bulk}$); $e$ = CPB voids ratio ($V_{void}/V_{solid}$); $G_{s-f}$ = pastefill specific gravity; $S_r$ = pastefill degree of saturation (varying from 0 to 1).

Figure 16 shows a typical variation of volumetric solids concentration ($C_{v\%}$) with solids concentration by mass ($C_{w\%}$) for five CPB mixes using five different tailings and one binding agent ($0.3 \times OPC + 0.7 \times GGBFS$) at 4.5 wt.%. The resultant paste backfill mixtures were poured into plastic moulds 10.125 cm (4 inches) in diameter and 20.5 cm (8 inches) in height or 7.62 cm (3 inches) in diameter and 15.24 cm (6 inches) in height, sealed, and cured in a humidity-controlled chamber at approximately 90–100% RH and 25°C (similar to underground mine working conditions). CPB samples were then subjected to compression tests at different curing periods.

### 4.2 CPB Preparation at a Backfill Plant

Figure 17 shows a typical flow chart for a backfill plant (Cayouette 2003). Final mill tailings are first fed into a high-capacity thickener to increase solids concentration from 35 wt.% to approximately

**Fig. 15** Typical variation of water-to-cement ratio w/c with paste backfill final mix solids concentration by mass ($C_{w\%}$) for four different binder contents ($B_{w\%}$) commonly used in the mining industry

**Fig. 16** Typical variation in volumetric solids concentration ($C_{V\%}$) with solids concentration by weight ($C_{w\%}$) for five CPB mixes using five different tailings and one binding agent (OPC-GGBFS) at 4.5 wt.% and 100% water saturation
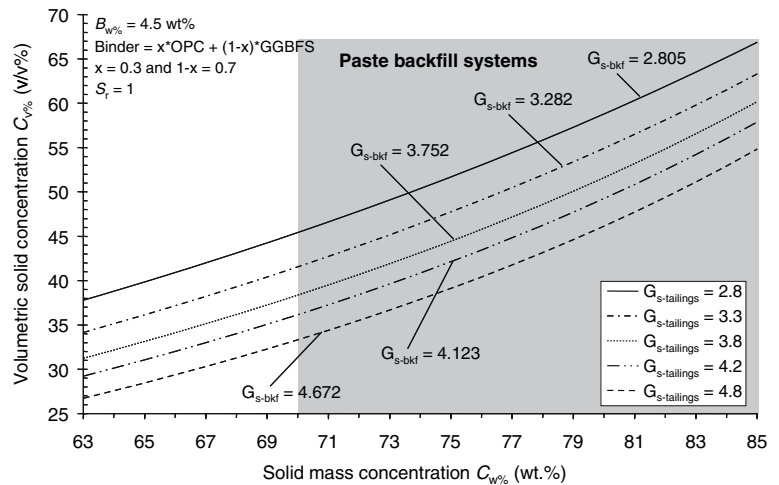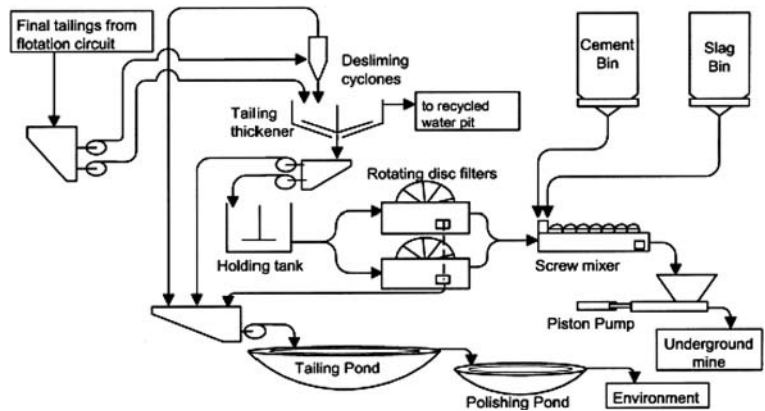


**Fig. 17** Paste backfill plant flow sheet at the Louvicourt mine, Canada (from Cayouette 2003)



55–60 wt.% by mass. Flocculent is added to aid filtration. The thickened tailings are then pumped from the thickener to a high-capacity holding tank (after cyanide destruction). From the surge tank, the thickened tailings are gravity-fed to disc filters operating alone or in parallel to produce filter cake with a solids concentration of approximately 70–82 wt.%. The filter cake is then discharged onto a belt (or reversible) conveyor and fed to a screw feeder for weighing. Finally, filter cake batches are mixed in a spiral (or screw) mixer with binder and water added for about 45 s to produce a paste with a specified consistency or slump height value S.

### 4.3 Importance of Controlling Tailings Density

Since binder proportion $B_{w\%}$ in the mix is calculated from tailings dry mass, the slightest variation in

tailings grain density $\rho_{s\text{-}t}$ produces an excess or loss-of-profit in binder proportioning. This variation of $\rho_{s\text{-}t}$ may be due to mineralogical changes in the ore body during stope extraction. Using a regression analysis on data taken from Benzaazoua and Bussière (1999) and Benzaazoua et al. (2000), and knowing total sulphur content %S (in percent), tailings grains specific density $\rho_{s\text{-}t}$ (in g/cm$^3$) is estimated using the following regression equation:

$$\rho_{s-t} = \frac{19.5674}{1 + 6.0094 \times \exp(-0.0072 * \%S)} \quad R = 0.9999$$

(34)

where $\rho_{s\text{-}t}$ is in g/cm$^3$; %S = tailings total sulphur content (wt.%).

For a given constant binder content $B_{w\%}$ (wt.%), increase in $\rho_{s\text{-}t}$ produces an increase in volumetric binder content $B_{v\%}$ (v/v%), and a reduction in $\rho_{s\text{-}t}$ produces a reduction in $B_{v\%}$, as described by Eq. 28.

### 4.3.1 Calculation of Adjusted Binder Content

To take into account the variation in tailings solid grains specific density $\rho_{s-t}$ in the mix design, adjusted binder content $B_{w\%-adj}$ (i.e., actual binder proportion used, not constant binder content, $B_{w\%-init}$) must be calculated using the following formula:

$$B_{w\%-adj} = B_{v\%-init}\left(\frac{\rho_{s-b}}{\rho_{s-t}}\right) = \frac{B_{w\%-init} \times (\rho_{s-t})_{init}}{\rho_{s-t}} \tag{35}$$

where $B_{v\%-init}$ = initial constant volumetric binder content (v/v%), corresponding to initial constant binder content by dry mass of tailings ($B_{w\%-init}$); $B_{w\%-init}$ = initial constant binder content by dry mass (wt.%); $\rho_{s-t}$ = current tailings solid particles density; $\rho_{s-b}$ = anhydrous binder particles density; and $(\rho_{s-t})_{init}$ = initial tailings solid particles density. Densities are in g/cm³, kg/m³ or tonne/m³.

Figure 18 presents a typical variation in adjusted binder content $B_{w\%-adj}$ with tailings grains density $\rho_{s-t}$, varying from the initial assumed value $((\rho_{s-t})_{init} = 3.85$ g/cm³). It shows that a decrease in tailings solid grains initial density $\rho_{s-t}$ produces a lack of binder content (loss-of-profit) with respect to adjusted binder content ($B_{w\%-adj}$), which leads in turn to under-proportioning of the binding agent in the final paste backfill mix. In contrast, an increase in $\rho_{s-t}$ produces excess binder content with respect to the adjusted binder content, which leads to over-proportioning of the binding agent, and therefore cost inefficiencies. However, under-proportioning of the binding agent causes the greater damage of reducing paste backfill strength development, while over-proportioning affects profits alone.

### 4.3.2 Calculation of Differential Binder Contents and Economic Implications

If adjusted binder content $B_{w\%-adj}$ is not considered, the result may be erroneous interpretation of the hypothetical influence of tailings solid grains density $\rho_{s-t}$ on paste backfill compressive strength development (e.g., Fall et al. 2004, 2005). Differential binder content ($\Delta B_{w\%}$) due to variations in tailings grains initial density $\rho_{s-t}$ (increase or decrease) is calculated with the following formula:

$$\Delta B_{w\%} = \left(B_{w\%-init} - B_{w\%-adj}\right)$$
$$= B_{w\%-init}\left(\frac{\rho_{s-t} - (\rho_{s-t})_{init}}{\rho_{s-t}}\right) \tag{36}$$

where $B_{w\%-init}$ = initial binder content (wt.%); $\rho_{s-t}$ = current tailings solid particles density; and $(\rho_{s-t})_{init}$ = initial tailings solid particles density. Densities are in g/cm³, kg/m³ or tonne/m³.

From Eq. 35, note that $\Delta B_{w\%}$ may be positive ($\Delta B_{w\%} > 0$) or negative ($\Delta B_{w\%} < 0$), depending on current tailings grains density $\rho_{s-t}$:

$$\begin{cases} \Delta B_{w\%}(>0) = B_{w\%-excess} & \text{if } \rho_{s-t} > (\rho_{s-t})_{init} \\ \Delta B_{w\%}(<0) = B_{w\%-lack} & \text{if } \rho_{s-t} < (\rho_{s-t})_{init} \end{cases} \tag{37}$$

where $B_{w\%-excess}$ = excess binder content (wt.%); $B_{w\%-lack}$ = lack of binder or loss-of-profit binder



**Fig. 18** Typical variation in adjusted binder content $B_{w\%-adj}$(wt%) with tailings grains density $\rho_{s-t}$, varying from the initial assumed value of 3.85 g/cm³ and for three different binder contents (3, 4.5, and 7 wt.%)
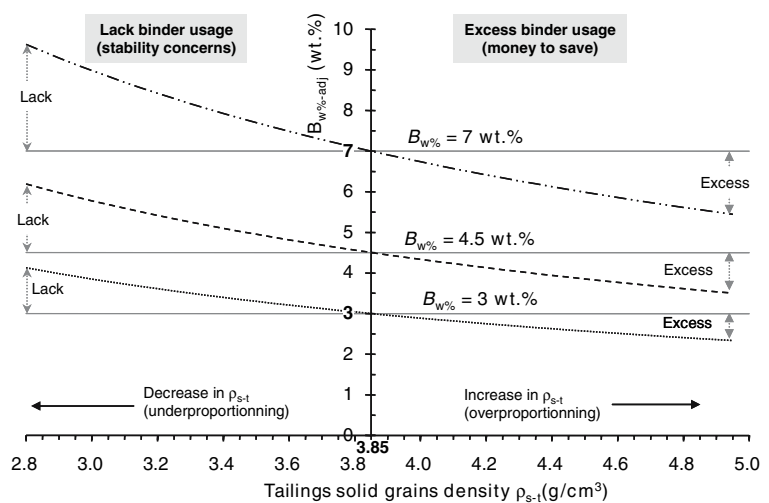
content, i.e., under-proportioned binding agent in the final mix.

Figure 19 presents typical variations in differential binder content ($\Delta B_{w\%}$) with tailings grains density ($\rho_{s-t}$), varying from the initial assumed value of 3.85 g/cm³. As shown, increased $\rho_{s-t}$ produces excess binder proportioning, while reduced $\rho_{s-t}$ produces under-proportioned (loss-of-profit) binder in the paste backfill mix.

Excess binder content ($B_{w\%-excess}$) may be converted into savings (if $B_{w\%-adj}$ is considered in the mix design) or loss (if $B_{w\%-adj}$ is not considered in the mix design), and annual savings or loss may be calculated as follows:

$$
\begin{aligned}
(\$/\text{year})_{\text{saved/lost}} \\
= \frac{M_{\text{dry-tailings}}(\text{tonne/year}) \times B_{w\%-excess}}{100} \\
\times (\$\text{binder/tonne})
\end{aligned}
\tag{38}
$$

where ($\$/\text{year})_{\text{saved/lost}}$ = money saved or lost per year if initial binder content is lower than the excess binder proportion; $M_{\text{dry-tailings}}$ = total mass of dry tailings used per year (tonne/year); $B_{w\%-excess}$ = excess binder content (wt.%); and ($\$\text{binder/tonne}$) = current cost of the binding agent.

To illustrate, consider an underground hard rock mine that uses $6 \times 10^5$ tonnes/year of total dry tailings having an initial solid grains density ($\rho_{s-t}$)$_{init}$ of 3,800 kg/m³ (3.8 tonnes/m³). Fixed constant binder content $B_{w\%-init}$ is 4.5 wt.% and solids concentration of the final mixes $C_{w\%}$ is 78%. The binder type used is a blended OPC-GGBFS at a ratio of 70:30 at a cost of 126.5 \$/tonne. Assuming a 7% increase in tailings solid density over the initial value

(i.e., $\rho_{s-t}$ = 4,050 kg/m³), savings would amount to about \$211k/year. With an approximately 16% increase (i.e., $\rho_{s-t}$ = 4,400 kg/m³), savings would amount to about \$466k/year (Fig. 20).

## 5 Paste Backfill Transportation

As defined above, paste backfill consists of the full size fraction of the tailings stream prepared as a high slurry density. The slurry behaves as a non-Newtonian fluid, meaning that it requires an applied force to commence flowing (Fig. 21). For example, toothpaste, a commonly used non-Newtonian fluid, must be squeezed (yield stress or applied load) to get the toothpaste out of the tube (Clark et al. 1995). Since backfill paste has higher viscosity, it exhibits plug flow when transported through a pipe. The outer portions of the slurry shear against the sidewall of the pipe while the central core travels as a plug (Grice 1998). Paste backfill flow in pipelines is entirely governed by its rheological properties. Rheology is the science of the flow and deformation of matter.

### 5.1 Rheological Models for Paste Backfill

The main method to achieve paste backfill flow in pipelines is the full-fall. Full-pipe occurs when the flowing paste forms a continuum with no air-filled gaps or discontinuities (vacuum "holes") in the pipeline segment under consideration (Li and Moerman 2002). The most fundamental relationship in the rheology of a non-Newtonian fluid is between shear rate, $\dot{\gamma}$ (s⁻¹) and pipe wall shear stress, $\tau_w$ (Pa). Once

**Fig. 19** Typical variation in differential binder content $\Delta B_{w\%}$ with tailings grains density $\rho_{s-t}$, varying from the initial assumed value of 3.85 g/cm³ and for three binder contents (3, 4.5 and 7 wt.%)
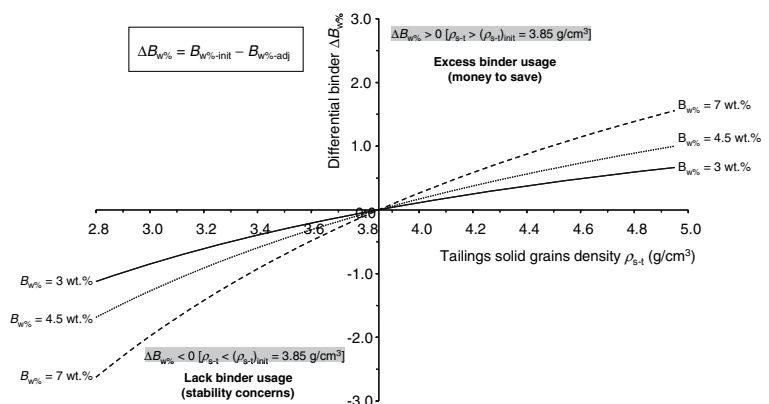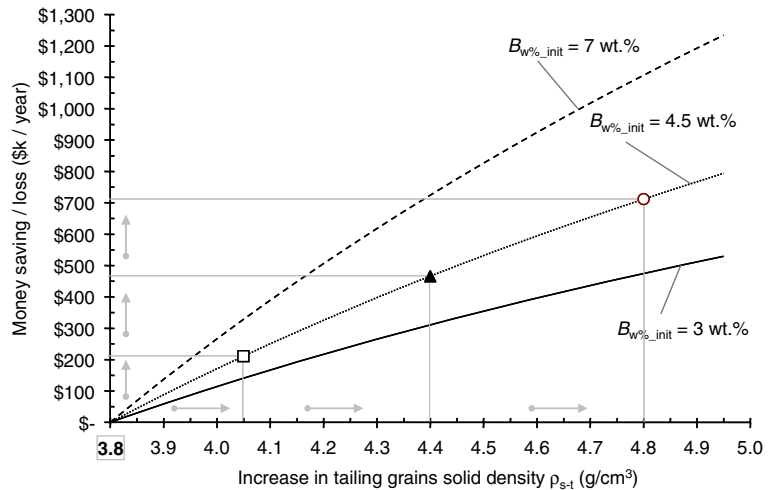
**Fig. 20** Example of money saved or lost according to increase in tailings solids density $\rho_{s-t}$ for three different binder contents (3, 4.5 and 7 wt.%)



this relationship is known, fluid behaviour in all flow situations can be deduced (e.g., viscosity and yield stress). The most frequently used fundamental non-Newtonain models to describe simple flow behaviour are the power law model, the Bingham model, and the Herschel–Bulkley model.

### 5.1.1 Power-law or Ostvald-de Waele Model

Many non-Newtonian materials undergo a simple increase or decrease in viscosity as shear rate increases. One of the most widely used forms of the general non-Newtonian constitutive law is a power-law (or Ostvald-de Waele) model, or two-parameter model, expressed as:

$$\tau_{w} = \eta_{app}\left(\frac{dV}{dr}\right)^{a} = \eta_{app}(\dot{\gamma})^{a} \tag{39}$$

where $\tau_{w}$ = wall shear stress (Pa); $\tau_{y}$ = shear yield stress (Pa); $\eta_{app}$ = non-Newtonian apparent viscosity
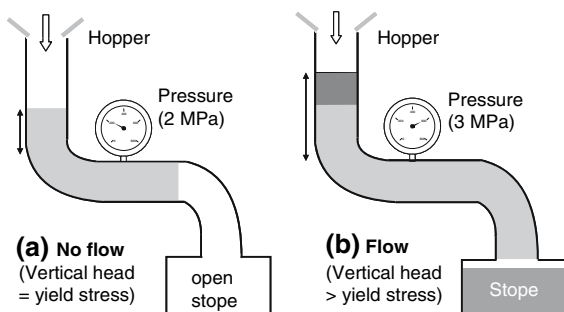


**Fig. 21** Schematic diagram of yield stress in paste backfill flowing through a pipeline (from Revell 2000)

defining fluid consistency (Pa s); $(dV/dr) = \dot{\gamma} =$ shear rate $(s^{-1})$ or velocity ratio $V$ (m/s); a point on the velocity profile $r$ (m); and $a$ = power-law model constant indicating the degree of non-Newtonian behaviour (the greater the departure from unity the more pronounced the non-Newtonian properties of the fluid). This model does not account for yield stress. If $a < 1$, a shear-thinning (or pseudoplastic) fluid is obtained, characterized by a progressively decreasing apparent viscosity with increasing shear rate. If $a > 1$, a shear-thickening (or dilatant) fluid in which apparent viscosity increases progressively with increasing shear rate is obtained. When $a = 1$, a Newtonian fluid is obtained.

### 5.1.2 Bingham Plastic Model

Some materials exhibit infinite viscosity until a sufficiently high stress is applied to initiate flow (yield stress). Above this stress, the material shows simple Newtonian flow. One of the simplest models covering viscoplastic fluids exhibiting such yield response is the ideal Bingham model (Fig. 22), expressed by the following two-parameter model:

$$\tau_{w} = \tau_{y} + \eta_{B}\frac{dV}{dr} = \tau_{y} + \eta_{B}\dot{\gamma} \tag{40}$$

where $\tau_{y}$ = shear yield stress (Pa); $\eta_{B}$ = Bingham plastic viscosity (Pa s); and $\dot{\gamma}$ = shear rate $(s^{-1})$. Basically, the Bingham model describes the viscosity characteristics of a fluid with yield stress when viscosity is independent of shear rate (constant). Therefore, the Bingham plastic model cannot account
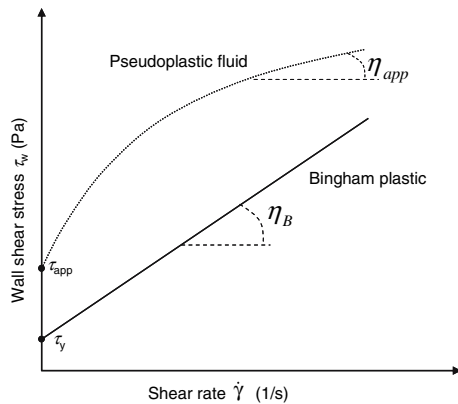
**Fig. 22** Rheograms for time-independent fluids

for the shear-thinning characteristics of general non-Newtonian fluids. Many concentrated particle suspensions and colloidal systems, such as mortar, concrete and possibly pastefill, show Bingham behaviour at low shear rates.

### 5.1.3 Herschel–Bulkley Model

The Herschel–Bulkley model is a three-parameter model used to describe viscoplastic materials exhibiting yield response with a shear-thinning relationship above yield stress (Fig. 22). This generalized model is a combination of the power law (Eq. 39) and Bingham models (Eq. 40), and is expressed by the following relationship:

$$\tau_w = \tau_{app} + \eta_{app}\left(\frac{dV}{dr}\right)^n = \tau_{app} + \eta_{app}(\dot{\gamma})^n \quad (41)$$

where $\tau_{app}$ = constant, interpreted as apparent shear yield stress (Pa); $\eta_{app}$ = consistency index or apparent viscosity (Pa s); $\dot{\gamma}$ = shear rate (s$^{-1}$); and $n$ = flow parameter indicating the degree of non-Newtonian behaviour (the greater the departure from unity the more pronounced the non-Newtonian properties of the fluid). When $n = 1$, the Herschel–Bulkley model is reduced to the Bingham model (Eq. 39). If $n < 1$, a pseudoplastic (or shear-thinning) fluid is obtained. If $n > 1$, a dilatant (or shear-thickening) fluid is obtained. The Herschel-Bulkley model is better fitted for many biological fluids, food products, and cosmetic products. Since this model tends to more realistically predict flow over a wider range of conditions than the Bingham model, it is

often applied to industrial fluids to specify design conditions for processing plants.

Since paste backfills are considered non-Newtonian fluids, their rheology is time-independent during pipeline transport. Most paste backfills show appreciable yield stress, and are therefore treated as Herschel–Bulkley fluids (Eq. 41). Some paste backfills are Bingham plastic in limited shear rate ranges. Others are yield pseudoplastic or yield dilatant, with the former more common than the latter (Li and Moerman 2002). Shear or apparent yield stress $\tau_y$ or $\tau_{app}$, apparent viscosity $\eta_{app}$, and flow parameters $a$ and $n$ are obtained by fitting Eqs. 39, 40 and 41 to a given flow curve or rheogram (shear rate-shear stress curve) obtained from rheometer tests (capillary, extrusion or rotational rheometer) using different tool geometries (vane, concentric cylinder, cone and plate, parallel plate, etc.).

### 5.1.4 Model for Plastic Fluid Flow Through a Pipe

For a Bingham plastic fluid such as pastefill, the relationship between pseudo shear rate $8V/D$ and shear stress at the pipe wall $\tau_w$ is given by:

$$\tau_w \approx \frac{\Delta PD}{4L}$$
$$= \eta_B \frac{8V}{D}\left[1 - \frac{4}{3}\left(\tau_y\frac{4L}{\Delta PD}\right) + \frac{1}{3}\left(\tau_y\frac{4L}{\Delta PD}\right)^4\right]^{-1}$$
$$(42)$$

where $\tau_y$ = shear yield stress (Pa); $\eta_B$ = Bingham plastic viscosity (Pa s); $\Delta P$ = pressure drop through a section of circular pipe of length $L$ (Pa); $D$ = pipe inner diameter (m); $L$ = pipe length (m); and $V$ = paste laminar velocity (m/s). Effective pipe inner diameter ($D$) for paste backfill transport ranges between 10 cm and 20 cm (4 and 8 inches). Paste flow velocity varies from 0.1 m/s to 1 m/s. The practical pumping distance of paste can reach 1,000 m longitudinally ($L_h$) and is unlimited vertically.

### 5.2 Standard Measurements of CPB Rheological Factors

In practice, it is not easy to obtain the true rheological properties of pastes, due to the complexity of the

experimental devices (rheometer tests). This makes it difficult or even impossible to determine or predict paste viscosity, which depends on several factors. Due to its simplicity, the standard slump test (used in the concrete industry) is widely used to determine paste backfill consistency. Slump is a measure of the drop in height of a material when released from a truncated metal cone that is open at both ends and sitting on a horizontal surface (Fig. 23). Slump determination allows characterizing the material's consistency in terms of transportability (Clark et al. 1995). According to Landriault et al. (1997), the optimum paste backfill slump to facilitate underground pumping is between 150 mm (6 inches) and 250 mm (10 inches).

Solids concentration $C_{w\%}$ is often used to compare mix compositions, particularly batches. To achieve mix consistency across batches, consistency can be measured by monitoring the electrical power used by the motor that turns the mixer paddles. The mixer is started and water is added until the power required by the motor reaches target for the mix consistency desired (Brackebusch 1994; Landriault and Lidkea 1993). The only requirement is that slump must be correlated to consistency and consistency correlated to power. Once the correlation between slump and pressure loss has been established, produced pressure gradient can be predicted.

### 5.3 Alternate Methods for Measuring Rheological Factors

To accurately define the rheology of paste backfill, both shear yield stress ($\tau_y$) and viscosity ($\mu$) must be measured. Most current tests measure only one rheological factor (i.e., slump height). The relationship between the factor measured and either of the

two fundamental rheological parameters is not obvious (Ferraris 1999). In most cases, $\tau_y$ and $\mu$ cannot be calculated from the measured factor, and are only assumed to be related. According to Ferraris (1999), slump, penetrating rod, and K-slump tests are related to shear yield stress ($\tau_y$), since they measure the paste's ability to start flowing. The remoulding test, LCL apparatus, vibrating testing apparatus, flow cone, turning tube viscometer, filling ability, and Orimet apparatus are related to viscosity because they measure the paste's ability to flow once applied stress (vibration or gravity) exceeds yield stress.

Slump height, an empirical measure of consistency, is dependent on both material yield stress and density, which are in turn dependent on chemical composition, particle specific gravity, and particle size. In the minerals industry, these factors may vary with changes in ore origin and processing. As a result, using slump height as the single parameter of consistency for paste backfill distribution systems potentially leads to problems (Clayton et al. 2003). Therefore, yield stress, a unique material property, is the preferred indicator of consistency. If slump height can be related to yield stress, the slump test offers a simple and ideal technique for on-site yield stress measurement (Clayton et al. 2003).

### 5.3.1 Direct Measurement of Yield Stress

Nguyen and Boger (1983, 1985) have suggested adapting the laboratory vane shear test to measure material yield stress ($\tau_y$). Test results allow obtaining a torque-angular deformation curve of material, where peak corresponds to maximum torque ($M_0$). Using the peak torque value and vane geometry



Fig. 23 Paste backfill consistency measurement by slump tests: (a) slump cone mould; (b) schematic view of the slump test (adapted from Ferraris and de Larrard 1998)
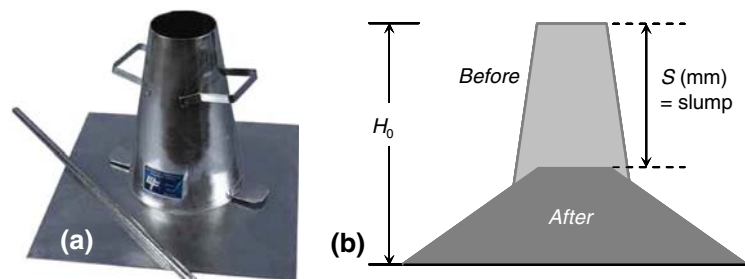
parameters, yield stress is calculated by the following relationship (Nguyen and Boger 1983, 1985):

$$\tau_y = \frac{M_0}{\frac{\pi D^3}{2}\left(\frac{H}{D} + \frac{1}{m+3}\right)} \quad (43)$$

where $\tau_y$ = paste yield stress (Pa); $M_0$ = maximum peak torque (N m); $D$ = vane diameter (m); $H$ = vane height (m); and $m$ = constant describing stress distribution over the cylinder (end effect): uniform distribution ($m = 0$) and non-uniform distribution ($m > 0$). Nguyen and Boger (1985) verified that the assumption of uniform stress distribution ($m = 0$) is valid.

Coussot and Boyer (1995) proposed a method to determine yield stress from the inclined plane test. The inclined plane used was a 1-m-long ($D$) channel with width $L$ varying between 5 cm and 25 cm and slope ($i$) varying between 10° and 30°. The bottom surface was plywood. The authors demonstrated that wall slip is negligible for mud flows on this surface type, and they successfully compared measured uniform flow depths ($h$) with theoretical predictions (based on rheometrical tests). They also observed no flow depth change when using surfaces with different roughness. Asymptotic depth ($h_0$), corresponding to at rest state (final position or equilibrium), leads to the determination of yield stress:

$$\tau_y = \rho g h_0 \sin(i) \quad (44)$$

where $\rho$ = material bulk density (kg/m³); $g$ = gravitational acceleration (m/s²); $h_0$ = final height of material (m); and $i$ = inclined plane slope angle.

Ulherr et al. (2002) developed a novel and simple method for measuring yield stress using a cylindrical penetrometer. Basically, static equilibrium of a falling penetrometer in a yield stress fluid (partial immersion) is measured, and uniform shear stress acting on the entire penetrometer surface is assumed. Yield stress is simply determined by a balance of forces acting on the penetrometer, as follows:

$$\tau_y = \frac{g\left[m_p - \rho \pi d^2 \left(\frac{l}{4} + \frac{d}{12}\right)\right]}{\pi d \left(l + \frac{\pi d}{8}\right)} \quad (45)$$

where $g$ = gravitational acceleration (m/s²); $m_p$ = total mass of the penetrometer (kg); $\rho$ = fluid bulk density (kg/m³); and $d$ and $l$ are the diameter (m) and immersed length (m) of the cylindrical section of the penetrometer.

Equation 45 indicates that yield stress is a function of the weight and dimensions of the immersed penetrometer. Thus, yield stress is readily determined by measuring equilibrium depth in the fluid for a penetrometer with known weight and diameter.

### 5.3.2 Analytical Models of Yield Stress and Slump

A number of analytical models have been developed to relate slump to a corresponding yield stress in order to predict slumping behaviour. The first analysis was made by Murata (1984), followed by Christensen (1991), who corrected a simple integration error made by Murata. Rajani and Morgenstern (1991) and Schowalter and Christensen (1998) further investigated the conical test. The slump test was first adapted to a cylindrical geometry by Chandler (1986) for application to the aluminium industry. Chandler realised there was a relationship between slump height and flow behaviour of the bauxite residue he was testing, but did not analytically relate the two. Pashias et al. (1996) developed a model for cylindrical geometry, for a favourable comparison of model and static vane test results. They also investigated slump height sensitivity to sample structure, material, aspect ratio, lift rate, and measurement time, and found slump measurement to be essentially independent of these factors.

These results were successfully validated by Clayton et al. (2003), Iveson and Franks (2003), Gawu and Fourie (2004), and Saak et al. (2004) for cylindrical moulds. Recently, Roussel and Coussot (2005) proposed an analytical correlation between spread and yield stress of cement pastes for the ASTM mini cone test, based on the work of Coussot et al. (1996). Roussel et al. (2005) correlated yield stress to slump or spread over a large range of yield stresses for any conical geometry. In addition, they quantified the influence of secondary phenomena such as surface forces, flow inertia, and initial cone shape on test meaningfulness.

Rajani and Morgenstern (1991) proposed a model to predict plastic yield stress $\tau_y$ from the ASTM C-143 slump cone height, based on both 2D (Tresca criterion) and 3D (von Mises criterion) yield criteria, as follows:

$$\tau_y = \frac{\rho g(H - h_0 - S)}{\beta \cdot \ln\left(\frac{7H^3}{(H+h_0)^3 - H^3}\right)} \qquad (46)$$

where $\rho$ = material bulk density (kg/m$^3$); $g$ = gravitational acceleration (m/s$^2$); $h_0$ = height of unyielded material (m or mm); $H$ = height of the ASTM C-143 slump cone ($H$ = 300 mm); $S$ = slump height (mm or m); and $\beta$ = constant depending on the yield criterion. $\beta = \sqrt{3}$ (von Mises) or 2 (Tresca). It should also be mentioned that $h_1 = H - h_0 - S$ and $h_0 = H - h_1 - S$.

Helmuth et al. (2006) developed a slump model based on geometric constraints for the standard ASTM C-143 concrete slump cone. Yield stress was calculated based on Murata's (1984) force balance approach, as follows:

$$\tau_y = \frac{\rho g V_c}{2\pi r_s^2} \qquad (47a)$$

and

$$r_s = \left(\sqrt{\frac{336}{(12-S)} - 3}\right) - 1 \qquad (47b)$$

where $\rho$ = material bulk density (kg/m$^3$); $g$ = gravitational acceleration (m/s$^2$); $V_c$ = cone or mould volume (m$^3$); $r_s$ = the radius of the slumped material base (m); and $S$ = slump height (m).

Pashias et al. (1996) adopted the slump test as a simple means to determine yield stress ($\tau_y$). They showed that slump height ($s$) measured by the modified slump test using an open-ended cylinder with an aspect ratio of 1 (diameter = height = 200 mm) could be directly related to yield stress, using the theory originally suggested by Murata (1984) and corrected by Christensen (1991). The relationship between slump height $s$ and yield stress is given by (Pashias et al. 1996):

$$\frac{s}{H} = 1 - \frac{2\tau_y}{\rho g H}\left[1 - \ln\left(\frac{2\tau_y}{\rho g H}\right)\right] \qquad (48a)$$

or

$$s' = 1 - 2\tau_y'\left[1 - \ln(2\tau_y')\right] \qquad (48b)$$

where $\rho$ = pastefill bulk density (kg/m$^3$); $g$ = gravitational acceleration (m/s$^2$); $s' = s/H$ = dimensionless slump; $s$ = cylindrical slump height (m); $\tau_y$ = shear yield stress obtained by the vane method (Pa);

$H$ = cylinder height (m); and $\tau_y' = \tau_y/\rho g H$ = dimensionless shear yield stress.

Iveson and Franks (2003) demonstrated that shear yield stress ($\tau_y$) of a paste-like suspension can be predicted by the modified slump method (Pashias et al. 1996), using the following analytical relationship:

$$\tau_y = \frac{\rho g H}{2}\left(1 - \sqrt{\frac{s}{H}}\right) \qquad (49)$$

where $\rho$ = paste-like suspension bulk density (kg/m$^3$); $g$ = gravitational acceleration (m/s$^2$); $H$ = slump cylinder height (m); and $s$ = cylinder slump height (m).

Clayton et al. (2003) proposed a general model relating slump height ($S$) and yield stress ($\tau_y$) to cone geometry. Thus, cylinder and cone geometries for slump measurement of the same material were compared. Predicted yield stress for the related cylinder model (Eq. 45) and cone model were compared to yield stress, determined using the well-established vane method (Nguyen and Boger 1983, 1985). The general cone model is given by:

$$s' = 1 - h_0' - 2\tau_y' \ln\left(\frac{\left(1 + \frac{1}{\alpha}\right)^3 - 1}{\left(1 + \frac{h_0'}{\alpha}\right)^3 - 1}\right) \qquad (50a)$$

with

$$\tau_y' = \frac{\alpha}{6}\left[\left(1 + \frac{h_0'}{\alpha}\right) - \frac{1}{\left(1 + \frac{h_0'}{\alpha}\right)^2}\right] \qquad (50b)$$

and

$$\alpha = \frac{R_0}{R_H - R_0} \qquad (50c)$$

where $\alpha$ = dimensionless quantity relating the top ($R_0$) and base ($R_H$) radii of the cone (when $R_H = 2R_0$, $\alpha = 1$, which is the case for the ASTM C-143 cone); $h_0'$ = dimensionless height of unyielded material; $\tau_y' = \tau_y/\rho g H$ = dimensionless shear yield stress; $\rho$ = material bulk density (kg/m$^3$); and $g$ = gravitational acceleration (m/s$^2$).

Saak et al. (2004) proposed a generalized model to determine yield stress by slump height from either cylindrical or conical geometries. This model may be

thought of as a combination of the Pashias et al. (Eq. 48) and Clayton et al. models (Eq. 50).

$$\begin{cases} \frac{s}{H} = 1 - \frac{h_0}{H} - \frac{h_1}{H} \\ \quad or \\ s' = 1 - h_0' - h_1' \end{cases} \tag{51a}$$

with

$$h_0 = 2H\tau_y + \frac{(2H\tau_y)^2}{a} + a - h_t \tag{51b}$$

$$h_1 = (2H\tau_y') \left[ Ln\left(\frac{H}{h_0}\right) + \ln\left(\frac{H^2 + 3h_t[H + h_t]}{h_0^2 + 3h_t[h_0 + h_t]}\right) \right] \tag{51c}$$

$$a = \sqrt[3]{\frac{h_t^3 + 16(H\tau_y)^3 + \sqrt{h_t^3 \left[ h_t^3 + 32(H\tau_y)^3 \right]}}{2}} \tag{51d}$$

$$h_t = H\left(\frac{r_t}{r_H - r}\right) \tag{51e}$$

And the dimensionless yield stress is given by:

$$\tau_y' = \left(\frac{1}{6H}\right) \left[ (h_0 + h_t) - \frac{(h_t)^3}{(h_0 + h_t)^2} \right] \tag{52}$$

where $r_t$ = radius at the slump cone top; $r_H$ = radius of the slump cone bottom; $h_t$ = height of the top cone section (untruncated cone); $\tau_y' = \tau_y/\rho g H$ = dimensionless shear yield stress; $H$ = slump cylinder height (m); $\rho$ = material bulk density (kg/m³); and $g$ = gravitational acceleration (m/s²).

Roussel and Coussot (2005) proposed analytical models relating shear yield stress to slump or spread over a large range of yield stresses for conical and cylindrical geometries. The models were defined for three asymptotic flow regimes: pure shear flow ($h \ll L$), pure elongation flow ($L \ll h$), and intermediate flow regime.

For the pure shear flow ($h \ll L$)

$$\tau_y' = h^{3/2}(1 - S')^{5/2} \sqrt{\frac{2\pi}{15V}} \tag{53a}$$

And as a function of spreading distance $L$, as follows:

$$\tau_y = \frac{225\rho g V^2}{128\pi^2 L^5} \tag{53b}$$

For pure elongation flow ($L \ll h$): von Mises yield criterion

$$\tau_y = \frac{\rho g(H - S - z_{cr})}{\sqrt{3}} \tag{54a}$$

Or in dimensionless form ($z_{cr} = 0$, valid for small slump $S' \ll 1$ only):

$$\tau_y' = \frac{\tau_y}{\rho g H} = \frac{(1 - S')}{\sqrt{3}} \tag{54b}$$

For an intermediate flow regime ($L \approx h$): von Mises yield criterion

$$S' = \frac{S}{H} = h' - \beta \left[ 1 + \ln\left(\frac{h'}{\beta}\right) \right] \tag{55}$$

Effect of tested fluid surface tension and contact angle.

For low shear yield stress, surface tension is non-negligible, and Eq. 53b can be rewritten to take into account surface tension and contact angle via a coefficient $\lambda$ ($\approx 0.005$), as follows:

$$\tau_y = \frac{1.747\rho V^2}{L^5} - \lambda \frac{L^2}{V} \tag{56}$$

where $h = H - s$ (m) and $L$ = final sample height and radius (m); $\tau_y$ = shear yield stress; $\tau_y' = \tau_y/\rho g H$ = dimensionless shear yield stress; $H$ = slump cylinder height (m); $s$ = slump height; $S'$ = dimensionless slump height (m); $\rho$ = material bulk density (kg/m³); $g$ = gravitational acceleration (m/s²); $V$ = sample volume (m³); $z_{cr}$ = critical flow stoppage height (m); $h'$ = dimensionless final height; and $\beta = \sqrt{3}$ (von Mises yield criterion).

### 5.3.3 Empirical and Semi-empirical Models of Yield Stress and Slump

Hu et al. (1996) found a semi-empirical correlation between yield stress $\tau_y$ (Pa) measured using a concrete rheometer, concrete bulk density $\rho$, and slump height $S$ (mm) for the ASTM C-143 slump cone, as follows:

$$\tau_y = \rho \left(\frac{300 - S}{270}\right) \tag{57}$$

where $\rho$ = concrete bulk density (kg/m³); $S$ = final slump height (mm); and 300 = height of the ASTM C-143 slump cone ($H$ = 300 mm). For paste backfill application, constant 270 must be calibrated.

Ferraris and de Larrard (1998) proposed a semi-empirical model between yield stress and slump height. From this model, shear yield stress ($\tau_y$) is calculated from final slump (S), using the following semi-empirical equation:

$$\tau_y = \rho\left(\frac{300 - S}{347}\right) + 212 \tag{58}$$

where $\rho$ = concrete bulk density (kg/m$^3$); S = final slump height (mm); and 300 = height of the ASTM C-143 cone (H = 300 mm). For paste backfill application, constants 347 and 212 must be calibrated.

Roussel (2006) proposed a semi-empirical model based on three-dimensional numerical simulations using a computational fluid dynamics Flow3D code. However, from the numerically predicted results, a simple linear approximation for slumps between 5 and 25 cm was proposed, as follows:

$$S = 25.5 - 17.6\frac{\tau_y}{\rho} \tag{59}$$

where $\tau_y$ = shear yield stress (Pa); $\rho$ = concrete bulk density (kg/m$^3$); S = final slump height (mm); and H/2 = 25.5, or half height of the mini cone (H = 50 mm). For paste backfill application, constant 17.6 must be calibrated.

### 5.3.4 Correlation between Yield Stress and Solids Concentration

Gawu and Fourie (2004) determined yield stress values on four thickened mineral tailings (with $G_{s\text{-}t}$ varying from 2.74 to 2.84) at varying solids concentrations by mass $C_{w\%}$ (from 20% to 72%), using the slump cylinder test proposed by Pashias et al. (1996), the rheometer test, and the miniature vane technique. An empirical relation developed from the slump cylinder test results appears to predict reasonably accurate yield stresses up to about 200 Pa, compared to vane and rheometer results. As a first approximation, they proposed a general regression equation describing change in yield stress ($\tau_0$) with solids concentration by mass ($C_{w\%}$), represented by the exponential relation:

$$\tau_0 = a_0 \exp(b_0 C_{w\%}) \tag{60}$$

where $a_0$ (Pa) and $b_0$ are experimentally determined constants. This exponential relation was also found in recent laboratory research on mineral tailings and paste backfill samples (Clayton 2003), where the constant $b_0$ was found to vary in the range $0.09 \leq b_0 \leq 0.96$.

Clayton (2003) in Grice (2005) proposed a power law model for paste backfill material made from gold tailings, as follows:

$$\tau_y = \alpha(C_w)^\beta \tag{61}$$

where $\alpha$ ($406 \times 10^3 \leq \alpha \leq 136 \times 10^4$) and $\beta$ ($20 \leq \beta \leq 25$) are experimentally determined material constants; and $C_w$ = backfill solids concentration by mass (in decimal).

### 5.3.5 Determination of Plastic Viscosity from the Modified Slump Test

Recently, a modified version of the standard slump cone test was developed to calculate concrete paste yield stress and viscosity (Ferraris and de Larrard 1998). As mentioned above, the standard slump test can only be correlated with shear yield stress ($\tau_y$). The modification consists of measuring not only final slump height (S), but also slumping time for the concrete (or CPB). The method consists of measuring the time (T) for a plate resting on the top of the concrete (or CPB) to slide down with the concrete (or CPB) a distance of 100 mm (Fig. 24).

For a range of concrete paste slump values (130–250 mm), viscosity is determined from the 100 mm slumping time (T), using an empirical equation developed by Ferraris and de Larrard (1998):

$$\eta = \alpha\rho T \tag{62}$$

where $\eta$ = plastic viscosity (Pa s); $\alpha$ = material constant (= 0.025 for concrete); $\rho$ = paste bulk density (kg/m$^3$); and T = slumping time (s).

### 5.4 Underground CPB Delivery Systems

According to Thomas et al. (1979), three possible systems may be used to transport material from a point on the surface to underground stopes, as shown in Fig. 21: *gravity/pumping*, *gravity*, and *pumping/gravity* systems.

- The *gravity/pumping* system has the advantage of being fully contained underground, thus causing no disruption to surface activities. Furthermore,

**Fig. 24** Schematic diagrams of the modified slump cone test based on measured slumping time $T$ (from Ferraris and de Larrard 1998)
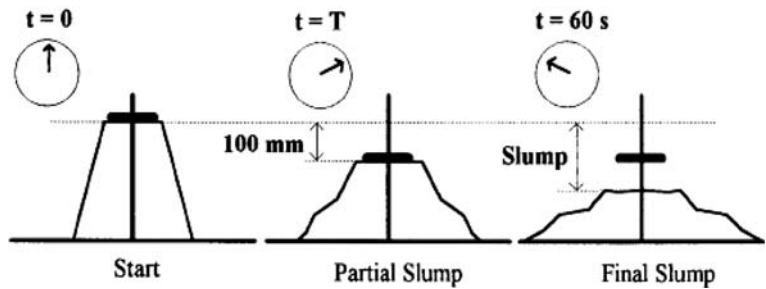


the vertical to horizontal distance ratio (V/H) is usually so favourable that little or no pumping energy is required.

- The *gravity* system (Fig. 25) has the advantage of progressively converting the vertical head to horizontal pressure, allowing shorter and lighter pipes to be used. Since take-off point pressures are moderate, line failures, if any, do not disrupt the main shaft or main operational level. The circuit can be developed progressively as the mine expands.

- The *pumping/gravity* system (Fig. 25) has the advantage of easy installation, inspection, and maintenance, with no special underground level requirements or disruption of the main shaft. However, the filling operation depends on a pumping operation with a long borehole for underground fill application, which requires a high-pressure take-off point.

### 5.5 Pipeline Flow of Paste Backfill

When paste backfill is delivered by pipeline to the disposal point in the stope, the friction factors



**Fig. 25** Basic configurations for paste backfill distribution systems (adapted from Thomas et al. 1979)

generated require high-pressure pipelines to transport the pastefill. Pressure is typically about 5 MPa for this type of laminar flow system. Early systems used high-pressure reciprocating pumps, but experience has shown that pastefill can be readily transported by gravity alone, provided that the reticulation geometry is favourable (Grice 1998).

#### 5.5.1 Paste Backfill Flow-loop Tests

For a given mine, paste backfill flow-loop tests using fully instrumented pipes must be performed to determine paste transport characteristics. Usually, an instrumented, closed-circuit pipeline system powered by a diesel engine positive-displacement pump is used. The instrumentation on the paste flow-loop tests provides essential engineering data such as flow rate ($Q$), friction head loss per unit length of pipe ($j = H/L$), shutdown and restart capabilities, and the power consumption required for full-scale pipeline designs. Figure 26 shows an example of paste flow-loop tests performed at the USBM's Spokane Research Center (Clark et al. 1995).

Calculation of friction head loss ($j$) allows determination of the running pressures of the paste distribution system: volumetric displacement pump type, choice of pipe diameter ($D$), flow rate ($Q$), and paste flow velocity ($V$). For a Bingham plastic fluid flowing in laminar regime (paste backfill), friction head loss or pressure gradient ($j$) is given by the following relationship:
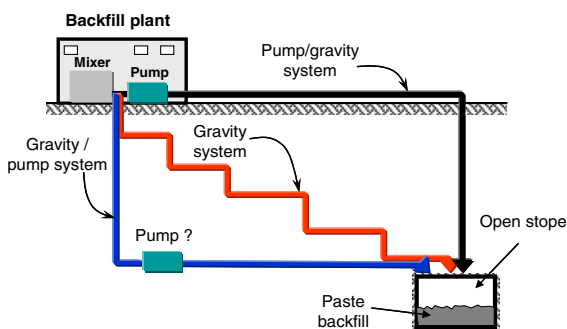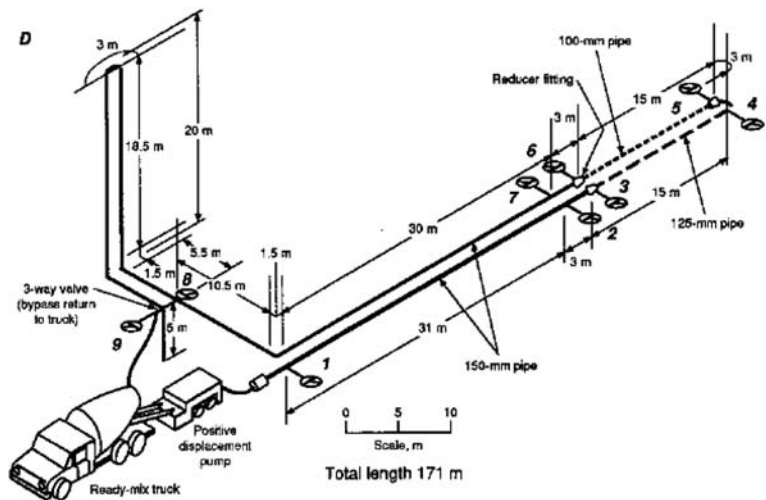
$$j = \frac{32V\eta_B}{D_i^2\left(1 - \frac{4}{3}\frac{\tau_w}{\tau_y} + \frac{1}{3}\left(\frac{\tau_w}{\tau_y}\right)^4\right)} \tag{63}$$

where $j$ = friction head loss or pressure gradient (Pa/m); $\eta_B$ = Bingham plastic viscosity (Pa s); $\tau_y$ = yield

**Fig. 26** Pastefill flow-loop tests and pressure monitoring locations (from Clark et al. 1995)



stress (Pa); $\tau_w$ = wall shear stress in Pa ($\tau_w \approx D_i \Delta P / 4L$); $D_i$ = pipe diameter (m); and $\Delta P$ = pressure drop (Pa).

It was observed that the pressure gradient ($j$) is higher for uncemented tailings than for paste backfill. This behaviour is directly related to tailings particle size distribution and pipe diameter. It was also observed that a decrease of half the $D_{50}$ value for initial tailings material could lead to a decrease of more than 45% of the pressure gradient (Clark et al. 1995). In addition, a substantial change in slump corresponds to a marginal variation of pastefill solid mass concentration, especially in the range 78–85 wt.%. Clark et al. (1995) observed that an increase of 45% in slump (increase of 5 cm) involved a decrease of 1% in solid mass concentration $C_{w\%}$ and 78 wt.% in pressure gradient.

As a rule of thumb, the pressure gradient for vertical flow or full-fall ($j_{vert}$) is approximately 66% of the pressure gradient measured during the flow loop test ($j_{loop}$). It is also assumed that the pressure gradient of a loop test is equal to $j$ during material pumping.

The use of rheological models such as Eqs. 39–43 and 63 requires a priori knowledge of apparent viscosity ($\eta_{app}$) or Bingham plastic viscosity ($\eta_B$), which is very difficult to predict, since it depends on several factors. It is therefore important to relate slump to plastic viscosity, as in Eq. 62 proposed by Ferraris and de Larrard (1998). Commonly used pipe diameters vary between 100 mm (4 inches) and 200 mm (8 inches). For example, paste backfill with

180-mm (7-inch) slump can be gravity fed at a flow rate of 100 tons/hour in a borehole/pipe system with a 150 mm (6 inches) diameter (Landriault et al. 1997).

### 5.5.2 Maximum Horizontal Flow Distance

The horizontal flow distance ($L_h$) generated by a standing column of material is obtained by dividing the pressure at the bottom of the standing column ($p_{bottom}$) by the frictional pressure gradient or pressure loss (Clark et al. 1995). The pressure at the bottom of a standing column is obtained by taking the difference between the pressure imparted by gravity and pressure lost through the frictional pressure gradient, so that the horizontal transport distance ($L_h$) is given by the following relationship (Fig. 27):
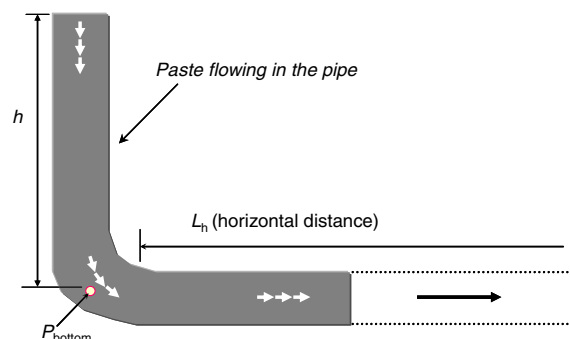


**Fig. 27** Schematic diagram of calculated horizontal distance of paste flow

$$L_h = \frac{p_{bottom}}{j} = \frac{(\gamma h - jh)}{j} = h\left(\frac{\gamma}{j} - 1\right) \qquad (64)$$

where $\gamma$ = fill bulk unit weight (kN/m$^3$); $h$ = maximum free-fall height of the paste in the pipe (m); and $j$ = friction head loss or pressure gradient (Pa/m). The maximum horizontal flow distance ($L_h$) and maximum vertical depth of the stope levels ($L_v$) define what is called the paste backfill distribution (or influence) cone.

## 6 Paste Backfill Placement in a Stope

Once all the transport parameters have been accurately determined, the paste backfill is delivered to underground openings through pipelines. Figure 28 presents a typical backfilled stope and the various components (fill mass, barricade, jointed rock mass, adjacent filled stope) as well as the stress field distribution.

After the stope is backfilled with CPB, the mechanical integrity can be threatened by several macroscopic factors (in opposition to the hydration process) that influence the mechanical strength of the CPB and the structural stability of the filled stope. These factors, which result from interactions between the CPB and rock walls (Aubertin et al. 2003; Li et al. 2003, 2005; Belem et al. 2004, 2006, 2007), are self-weight consolidation settlement of the fill due to partial drainage (Belem et al. 2006, 2007), stope volume, stress field distribution within the backfill mass (pressures at the stope floor and on the barricade), wall convergence against the fill mass,
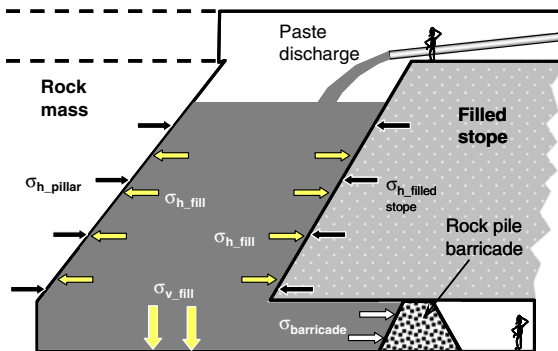


**Fig. 28** Schematic diagram of backfilled stope components and stress field distribution

shrinkage, and arching effects (Aubertin et al. 2003; Li et al. 2003; Belem et al. 2004).

Drainage and settlement are conducive to CPB hardening (Belem et al. 2001, 2002, 2006). On the other hand, the fill mass achieves stability due to the development of arching effects, depending on stope dimensions.

When excessive, pressures at the stope floor and on the barricade exert a harmful effect on the stability of the filled stope. Consequently, the factors that influence stope stability must be understood to ensure better ground control (Belem et al. 2004). Knowledge of the magnitude of pressures on the barricade allows better planning of the extraction sequences. Knowledge of the stress field within the fill mass facilitates the stability analysis when either one face is exposed or when a gallery to access a new ore body must be excavated through the CPB mass.

## 7 Conclusions

This paper provides an overview of the design and application of paste backfill in underground hard rock mines. When applying paste backfill, the limiting strength and pressures that develop in the fill mass must be determined according to the geometry of the opened stopes and initial stress conditions. To meet these criteria, laboratory optimization of paste backfill mix design is essential to determine the optimal mixture to achieve the desired limiting strength. In addition, before beginning stope filling, the rheological properties of the fill material must be known. To do so, a rheological model of paste backfill behaviour (Bingham or Pseudo-plastic) can be selected to determine two essential parameters: yield stress ($\tau_y$) and plastic viscosity ($\eta$).

Paste backfill pumpability can also be determined using standard or modified ASTM slump tests. Modified tests allow relating slump and *slumping time* ($T$) to yield stress ($\tau_y$) and plastic viscosity ($\eta$). Depending on the mine's distribution system (e.g., gravity, pumping, etc.), paste flow-loop tests are required to estimate the friction head loss or pressure gradient ($j$) to be used to design and implement pipeline reticulation in order to better control operating pressures. Moreover, knowing the pressure gradient $j$, maximum horizontal distance for paste flow with no additional pressure (flow distribution or

influence cone) can be calculated. Once the paste backfill is transported underground by pipeline to the open stopes, it interacts with the stopes and pillar walls, and the initial physical and mechanical properties evolve during curing.

# References

Arioglu E (1983) Design of supports in mines. Wiley and Sons, New York, 248 pp

Arioglu E (1984) Design aspects of cemented aggregate fill mixes for tungsten stoping operations. J Min Sci Technol 1(3):209–214

Askew JE, McCarthy PL, Fitzerald DJ (1978) Backfill research for pillar extraction at ZC/NBHC. In: Proceedings of 12th Canadian rock mechanics symposium, pp 100–110

ASTM Designation C-143-90 (1996) Standard test method for slump of hydraulic cement concrete. Annual Book of ASTM Standards, 04.01, American Society for Testing and Material, Easton, MD, pp 85–87

Aubertin M, Li L, Arnoldi S, Belem T, Bussière B, Benzaazoua M, Simon R (2003) Interaction between backfill and rock mass in narrow stopes. In: Proceedings of 12th Pan-american conference on soil mechanics and geotechnical engineering and 39th U.S. rock mechanics symposium, 22–26 June, Boston, Massachusetts, USA, vol 1, Verlag Gückauf GmbH, Essen, pp 1157–1164

Barret JR, Coulthard MA, Dight PM (1978) Determination of fill stability, mining with backfill. In: Proceedings of 12th Canadian rock mechanics symposium, Canadian Institute of Mining and Metallurgy, Quebec, Special vol 19, pp 85–91

Belem T, Benzaazoua M, Bussière B (2000) Mechanical behaviour of cemented paste backfill. In: Proceedings of 53th Canadian geotechnical conference. Geotechnical Engineering at the dawn of the third millennium. 15–18 October, Montreal, vol 1, pp 373–380

Belem T, Benzaazoua M, Bussière B, Dagenais AM (2002) Effects of settlement and drainage on strength development within mine paste backfill. In: Proceedings of tailings and mine waste'02, 27–30 January, Fort Collins, Colorado. Balkema, Rotterdam, pp 139–148

Belem T, Bussière B, Benzaazoua M, (2001) The effect of microstructural evolution on the physical properties of paste backfill. In: Proceedings of tailings and mine waste'01, January 16–19, Fort Collins, Colorado. A.A. Balkema, Rotterdam, pp 365–374

Belem T, El-Aatar O, Bussière B, Benzaazoua M, Fall M, Yilmaz E (2006) Characterization of self-weight consolidated paste backfill. In: Jewell R, Lawson S, Newman Ph (eds) Proceedings of 9th international seminar on paste and thickened tailings—paste'06, 3–7 April. Limerick, Ireland, pp 333–345

Belem T, El-Aatar O, Benzaazoua M, Bussière B, Yilmaz E (2007) Hydro-geotechnical and geochemical characterization of column consolidated cemented paste backfill. In: Proceedings of 9th International Symposium in Mining with Backfill, April 29 to May 2, 2007, Montreal, Canada, CIM, Paper No. 2523, 10 pp

Belem T, Harvey A, Simon R, Aubertin M (2004) Measurement and prediction of internal stresses in an underground opening during its filling with cemented fill. In: Villaescusa E, Potvin Y (eds) Proceedings of the fifth international symposium on ground support in mining and underground construction, 28–30 September. Perth, Western Australia, Australia, Tayler & Francis Group, London, pp 619–630

Bellmann F, Möser B, Stark J (2006) Influence of sulphate solution concentration on the formation of gypsum in sulfate resistance test specimen. Cement Concrete Res 36:358–363

Benzaazoua M, Belem T (2000) Optimization of sulfide-rich paste backfill mixtures for increasing long-term strength and stability. In: Sánchez MA, Vergara F, Castro SH (eds) Proceedings of fifth conference on clean technology for mining industry, Santiago, University of Concepción, vol I, pp 343–352

Benzaazoua M, Belem T, Jolette D (2000) Investigation de la stabilité chimique et de son impact sur la qualité des remblais miniers cimentés. In: IRSST Report No. R-260, 172 pp

Benzaazoua M, Belem T, Bussière B (2002) Chemical aspect of sulfurous paste backfill mixtures. Cement Concrete Res 32(7):1133–1144

Benzaazoua M, Belem T, Ouellet S, Fall M (2003) Utilisation du remblai en pâte comme support de terrain. Partie II: comportement a court, a moyen et a long terme. In: Proceedings of Après-mines 2003. Impacts et gestion des risques: besoins et acquis de la recherche, 5–7 February. Nancy, GISOS, CD-ROM, 12 pp

Benzaazoua M, Bussière B (1999) Desulphurization of tailings with low neutralization potential: kinetic study and flotation modeling. In: Goldsack P, Belzile N, Yearwood P, Hall G (eds) Proceedings of Sudbury'99, mining and the environment II, vol 1, pp 29–38

Benzaazoua M, Fall M, Belem T (2004) A contribution to understanding the hardening process of cemented paste-fill. Miner Eng 17(2):141–152

Benzaazoua M, Ouellet J, Servant S, Newman P, Verburg R (1999) Cementitious backfill with high sulfur content: physical, chemical and mineralogical characterization. Cement Concrete Res 29:719–725

Brackebusch FW (1994) Basics of paste backfill systems. Miner Eng 46:1175–1178

Brooker EH, Ireland HO (1965) Earth pressures at rest related to stress history. Can Geotech J 2(1):1–15

Cai S (1983) A simple and convenient method for design of strength of cemented hydraulic fill. In: Proceedings of international symposium on mining with backfill. A.A. Balkema, Rotterdam, pp 405–412

Cayouette J (2003) Optimization of the paste backfill plant at Louvicourt mine. CIM Bull 96(1075):51–57

Chandler JL (1986) The stacking and solar drying process for disposal of bauxite tailings in Jamaica. In: Proceedings of the international conference on bauxite tailings, Kingston, Jamaica, Jamaica Bauxite Institute, University of the West Indies, pp 101–105

Chen L, Jiao D (1991) A design procedure for cemented fill for open stoping operations. J Min Sci Tech 12:333–343

Christensen G (1991) Modelling the flow of fresh concrete: the slump test. Ph.D. Thesis, Princeton University, Princeton, NJ, USA

Clark CC, Vickery JD, Backer RR (1995) Transport of total tailings paste backfill: results of full-scale pipe test loop pumping tests. Report of investigation, RI 9573, USBM, 37 pp

Clayton S (2003) The importance of rheology in pastefill operations. Ph.D. thesis, University of Melbourne

Clayton S, Grice TG, Boger DV (2003) Analysis of the slump test for on-site yield stress measurement of mineral suspensions. Int J Miner Process 70:3–21

Coates DF (1981) Caving, Subsidence, and Ground Control. In: Rock Mechanics Principles, CANMET, Department of Energy, Mines and Resources, Canada, Chapter 5, pp 5.1–5.42

Coussot P, Boyer S (1995) Determination of yield stress fluid behaviour from inclined plane test. Rheologica Acta 34:534–543

Coussot P, Proust S, Ancey C (1996) Rheological interpretation of deposits of yield stress fluids. J Non-Newtonian Fluid Mech 66:55–70

Craig RF (1995) Soil mechanics, 5th edn. Chapman and Hill Publishing, London, 427 pp

Donovan JG (1999) The effects of backfilling on ground control and recovery in thin-seam coal mining, M.Sc. Thesis, Virginia Polytechnic Institute and State University, Blacksburg, Virginia, 148 pp

Douglas E, Malhotra VM (1989) Ground granulated blast furnace slag for cemented mine backfill: production and evaluation. CIM Bull 82(929):27–36

Fall M, Benzaazoua M (2003) Advances in predicting performance properties and cost of paste backfill. In: Proceedings on tailings and mine waste'03, October 12–15, Vail, USA, Balkema, Rotterdam, pp 73–85

Fall M, Benzaazoua M, Ouellet S (2004) Effect of tailings properties on paste backfill performance. In: Proceedings of the eight international symposium on mining with backfill, September 2004, Beijing, The Nonferrous Metals Society of China, pp 193–202

Fall M, Benzaazoua M, Ouellet S (2005) Experimental characterization of the influence of tailings fineness and density on the quality of cemented paste backfill. Min Eng 18:41–44

Ferraris CF (1999) Measurement of the rheological properties of high performance concrete: state of the art report. J Res Natl Inst Stand Technol 104:461–478

Ferraris CF, de Larrard F (1998) Modified slump test to measure rheological parameters of fresh concrete. Cement Concrete Aggr 20(2):241–247

Gawu SKY, Fourie AB (2004) Assessment of the modified slump test as a measure of the yield stress of high-density thickened tailings. Can Geotech J 41:39–47

Grice AG (1998) Underground mining with backfill, The 2nd Annual Summit—Mine Tailings Disposal Systems, 24–25 November 1998, Brisbane, Australia, 14 pp

Grice AG (2001) Recent minefill developments in Australia. In: Proceedings of seventh international symposium on mining with backfill, Minefill 2001, SME, Seatle, Washington, pp 351–357

Grice AG (2005) In: Potvin Y, Thomas EG, Fourie AB (eds) Handbook on mine fill. Australian Centre for Geomechanics, University of Western Australia, Chapter 4, pp 50–63

Guang-Xu T, Mao-Yuan H (1983) Assessment on support ability of the fill mass. In: Proceedings of international symposium on mining with backfill, A.A. Balkema, Rotterdam, pp 433–442

Hansen JB (1968) A revised extended formula for bearing capacity. Danish Geotechnical Institute Bulletin, No. 28

Hassani F, Archibald JH (1998) Mine backfill. CIM, CD-ROM

Hassani F, Bois D (1992) Economic and technical feasibility for backfill design in Quebec underground mines. Final report 1/2, Canada-Quebec Mineral Development Agreement, Research & Development in Quebec Mines. Contract no. EADM 1989–1992, File no. 71226002

Helmuth RA, Hills LM, Whiting DA, Bhattacharja S (2006) Abnormal concrete performance in the presence of admixtures, Report 2006, Portland Cement Association, Skokie, IL, USA

Hu C, de Larrard F, Sedran T, Boulay C, Bosc F, Deflorenne F (1996) Validation of BTRHEOM, the newrheometer for soft-to-fluid concrete. Mater Struct RILEM 29(194):620–631

Hunt RE (1986) Geotechnical engineering analysis and evaluation. McGraw Hill, New York, 729 pp

Iveson SM, Franks GV (2003) Particle technology demonstrations for the classroom and laboratory. Chemical Engineering Education, ChE Division of ASEE 274–280

Jaky J (1944) The coefficient of earth pressure at rest. J Soc Hung Architects Eng 78:355–358

Kesimal A, Ercikdi B, Yilmaz E (2003) The effect of desliming by sedimentation on paste backfill performance. Min Eng 16:1009–1011

Landriault DA, Lidkea W (1993) Paste fill and high density slurry fill. In: Proceedings of the international congress on mine design, Queens University, Kingston, Ontario, Canada, August

Landriault DA, Verburg R, Cincilla W, Welch D (1997) Paste technology for underground backfill and surface tailings disposal applications. Short course notes, Canadian Institute of Mining and Metallurgy, Technical workshop—April 27, Vancouver, British Columbia, Canada, 120 pp

Lawrence CD (1992) The influence of binder type on sulfate resistance. Cement Concrete Res 22:1047–1058

le Roux KA, Bawden WF, Grabinsky MWF (2002) Assessing the interaction between hydration rate and fill rate for a cemented paste backfill. In: Proceedings of the 55th Canadian geotechnical and 3rd joint IAH-CNC groundwater specialty conferences. Niagara Falls, Ontario, 20–23 October, pp 427–432

Li L, Aubertin M, Simon R, Bussière B, Belem T (2003) Modeling arching effects in narrow backfilled stopes with

FLAC. In: Proceedings of 3rd international FLAC symposium, May 31, 2003, Sudbury, A.A. Balkema, Rotterdam, pp 211–218

Li L, Aubertin M, Belem T (2005) Formulation of a three dimensional analytical solution to evaluate stresses in backfilled vertical narrow openings. Can Geotech J 42:1705–1717

Li M, Moerman A (2002) Perspectives on the scientific and engineering principles underlying flow of mineral pastes. In: Proceedings 34th annual meeting of CMP, Ottawa, Canada, Paper No. 35, pp 573–595

Li T, Singh U, Coxon J, Grice TG, Sainsbury D (2002) Development and application of paste fill using dry tailings. First International Seminar on Deep and High Stress Mining, Perth, 10 pp

Marston A (1930) The theory of external loads on closed conduits in the light of latest experiments. Bulletin No. 96, Iowa Engineering Experiment Station, Ames, Iowa

Mitchell RJ (1983) Earth structures engineering, Chapter 6. Allen & Unwin, London

Mitchell RJ (1989a) Stability of cemented tailings backfill. Computer and physical modelling in geotechnical engineering. Balkema, Rotterdam, pp 501–507

Mitchell RJ (1989b) Model studies on the stability of confined fills. Can Geotech J 26:210–216

Mitchell RJ, Olsen RS, Smith JD (1982) Model studies on cemented tailings used in mine backfill. Can Geotech J 19(1):14–28

Mitchell RJ, Roettger JJ (1989) Analysis and modelling of sill pillars. Innovations in mining backfill technology. Balkema, Rotterdam, pp 53–62

Murata J (1984) Flow and deformation of fresh concrete. Mater Construct 17:117–129

Nantel J (1998) Recent developments and trends in backfill practices in Canada. In: Proceedings of the sixth international symposium on mining with backfill, Minefill '98, AIMM, Brisbane, pp 11–14

Naylor J, Farmery RA, Tenbergen RA (1997) Paste backfill at the Macassa mine with flash paste production in a paste production and storage mechanism. In: Proceedings 29th annual meeting of the Canadian mineral processors, Ottawa, Ontario, January 21–23, pp 408–420

Nguyen QD, Boger DV (1983) Yield stress measurement for concentrated suspensions. J Rheol 27:321–349

Nguyen QD, Boger DV (1985) Direct yield stress measurement with the vane method. J Rheol 29:335–347

Pashias N, Boger DV, Summers J, Glenister DJ (1996) A fifty cent rheometer for yield stress measurements. J Rheol 40(6):1179–1189

Rajani B, Morgenstern N (1991) On the yield stress of geotechnical materials from the slump test. Can Geotech J 28:457–462

Revell M (2000) Cannington backfill taking the pig out of paste. Paste Technology Seminar, April 2000, Perth, Australia, pp 1–12

Roussel N (2006) Correlation between yield stress and slump: comparison between numerical simulations and concrete rheometers results. Mater Struct 39:501–509

Roussel N, Coussot P (2005) "Fifty-cent rheometer" for yield stress measurements: from slump to spreading flow. J Rheol 49(3):705–718

Roussel N, Stefani C, Le Roy R (2005) From minicone test to Abrams cone test: measurement of cement based materials yield stress using slump test. Cement Concrete Res 35:817–822

Saak AW, Jennings HM, Shah SP (2004) A generalized approach for the determination of yield stress by slump and slump flow. Cement Concrete Res 34:363–371

Schowalter WR, Christensen G (1998) Toward a rationalization of the slump test for fresh concrete: comparisons of calculations and experiments. J Rheol 42:865–870

Smith JD, Dejongh CL, Mitchell RJ (1983) Large scale model tests to determine backfill strength requirements for pillar recovery at the Black Mountain Mine. In: Proceedings of international symposium on mining with backfill, Lulea, June 7–9, pp 413–423

Stone DMR (1993) The optimization of mix designs for cemented rockfill. In: Proceedings of fifth international symposium on mining with backfill, MINEFILL'93, Johannesbourg, SAIMM, pp 249–253

Terzaghi K (1943) Theoretical soil mechanics. John Wiley & Sons, New York

Thomas EG, Nantel, JH, Notely KR (1979) Fill technology in underground metalliferous mines. International Academic Services Limited, Canada, 293 pp

Uhlherr PHT, Guo J, Fang T-N, Tiu C (2002) Static measurement of yield stress using a cylindrical penetrometer. Korea-Australia Rheol J 14:17–23

Van Horn AD (1963) A study of loads on underground structures, part III. Iowa Engineering Experiment Station

Wang C, Villaescusa E (2001) Influence of water salinity on the properties of cemented tailings backfill. Min Technol: IMM Trans Sect A 110(1):62–65

Wayment WR (1978) Backfilling with tailings—a new approach. In: Proceedings of 12th Canadian rock mechanics symposium, mining with backfill. Canadian Institute of Mining and Metallurgy, Quebec, Special Vol 19, pp 111–116

Yilmaz E, Kesimal A, Ercikdi B (2004) Strength development of paste backfill samples at long term using two different binders. In: Proceedings of the 8th symposium on mining with backfill, pp 281–285

Yu TR (1992) Mechanisms of fill failure and fill strength requirements. In: Proceedings of 6th Canadian rock mechanics symposium, pp 1–6